Departamento de Ciências e Tecnologias de Informação

Characterization of a Global 4G Mobile Communications Network Using the Commercial Aircraft Network

Ana Gisela Duarte Madruga

Dissertation presented in partial fulfilment of the requirements for the degree

Master in Telecommunications and Computer Engineering

Supervisor:

PhD. Pedro Joaquim Amaro Sebastião

Co-Supervisor:

PhD. Américo Manuel Carapeto Correia

September 2019

Acknowledgments

Firstly, I would like to thank my supervisor Prof. Pedro Sebastião and co-supervisor Prof. Américo Correia for the patience and guidance during the time I was writing this dissertation. A very special thank you to Prof. Pedro Sebastião for the support in this final stage. It was truly meaningful and crucial to accomplish the delivery of this dissertation and I am gratefully indebted.

I would also like to thank my family, my friends and colleagues from ISCTE-IUL for the friendship and for believing and encouraging me.

Last, but not least, I would also like to express my gratitude to my beloved Pedro for providing me with unfailing support and continuous encouragement. Thank you.

Abstract

The ever increasing demand for high data rates and mobility, at the same time with the lowest latency possible, comes as a motivation and inspiration for the writing of this dissertation.

Besides terrestrial networks, another common way to communicate nowadays is via satellite networks; low Earth orbit satellites are the ones closer to the Earth, still, they are 800km away, requiring high energetic consumption.

Routes used by commercial air traffic cover great part of the globe, with higher incidence in the most populated areas, namely North America, Europe and Eastern Asia.

The main objective of this project is to prove that it would be possible to have a global coverage network or, at least, a network able to fulfil the needs of users located in the most populated regions, where air traffic is denser. Users would be able to communicate to any part of the world; the nearest aircraft gets the signal and, since they are organized as a mesh network, it travels from aircraft to aircraft until it reaches its final destination.

LTE frequency bands have a great margin to operate without interfering with the frequencies used in aeronautical radio communication systems, as will be seen in Chapter 3.

The work developed shows that the most favourable conditions regarding the maximum distances obtained to establish the communication will be to set up the proposed system using QPSK, a 1.4 MHz channel and transmission frequency should be 737 MHz. Thus, maximum attainable distance in rural scenario is 46.62 km.

Keywords

Global communications network, commercial aircrafts, LTE, attenuation, propagation model

Resumo

A constante procura por taxas de alto débito e mobilidade, aliado à menor latência possível, surgiram como motivação e inspiração para a escrita desta dissertação.

Além das redes terrestres, outra forma comum de comunicar nos dias de hoje é recorrendo a redes de satélites; os satélites de baixa órbita são os que estão mais próximo da Terra, no entanto estão a 800km de distância, o que requer um elevado consumo energético.

As rotas utilizadas pelos aviões comerciais cobrem grande parte do globo, com maior incidência nas zonas mais povoadas, nomeadamente América do Norte, Europa e Este da Asia.

O maior objetivo deste projeto é provar que é possível haver uma rede de cobertura global ou, pelo menos, uma rede capaz de satisfazer as necessidades dos utilizadores localizados nas zonas mais povoadas onde o tráfego aéreo é mais frequente. Os utilizadores poderiam comunicar para qualquer parte do mundo; o avião mais próximo receberia o sinal e, como estes estão organizados numa rede *mesh*, o sinal viajaria de avião em avião, até chegar ao seu destino.

As bandas de frequência usadas no LTE têm uma grande margem para operar sem interferir com as frequências utilizadas nas comunicações na aviação, como será visto no Capítulo 3.

O trabalho desenvolvido mostra-nos que as condições mais favoráveis, no que toca a distâncias máximas obtidas para estabelecer a comunicação, serão montar o sistema proposto utilizando QPSK, um canal de 1.4 MHz e cuja frequência de transmissão seja 737 MHz. Assim, consegue-se obter uma distância máxima de transmissão em ambiente rural de 46.62 km.

Palavras-chave

Rede de comunicações global, aviação comercial, LTE, atenuação, modelo de propagação

List of figures

List of tables

List of acronyms

1G – 1st Generation

2G – 2nd Generation

3G – 3rd Generation

3GPP – 3rd Generation Partnership Project

4G – 4th Generation

ADC – Analogue to Digital Converter

BS – Base Station

CN – Core Network

CoMP – Coordinated Multipoint

CP – Cyclic Prefix

EIRP – Equivalent Isotropic Radiated Power

eNB – eNode-B

EPC – Evolved Packet Core

EPS – Evolved Packet System

E-UTRAN – Evolved-UMTS Terrestrial Radio Access Network

FDD – Frequency Division Duplex

FDM – Frequency Division Multiplexing

FFT – Fast Fourier Transform

GSM – Global System for Mobile Communications

HSPA – High Speed Packet Access

ICAO – International Civil Aviation Organization

IFFT – Inverse Fast Fourier Transform

IM – Implementation Margin

IP – Internet Protocol

ISDN – Integrated Services Digital Network

ISI – Inter-Symbol Interference

ITU – International Telecommunication Union

LoS – Line of Sight

LTE – Long Term Evolution

LTE-A – Long Term Evolution – Advanced

MIMO – Multiple Input Multiple Output

MME – Mobility Management Entity

MU-MIMO – Multiple User - Multiple Input Multiple Output

NF – Noise Figure

OFDM – Orthogonal Frequency Division Multiplexing

OFDMA – Orthogonal Frequency Division Multiple Access

PAPR – Peak-to-Average Power Ratio

PDN – Packet Data Network

P-GW – PDN Gateway

QAM – Quadrature Amplitude Modulation

QoS – Quality of Service

QPSK – Quadrature Phase Shift Keying

RAN – Radio Access Network

REFSENS – Reference Sensitivity

SAE – System Architecture Evolution

SC-FDMA – Single Carrier Frequency Division Multiple Access

SDMA – Spatial Division Multiple Access

S-GW – Serving Gateway

SINR – Signal to Interference plus Noise Ratio

SON – Self Organized Network

TDD – Time Division Duplex

UE – User Equipment

UMTS – Universal Mobile Telecommunications System

WCDMA – Wide-Band Code-Division Multiple Access

Contents

Chapter 1

Introduction

In this chapter, the motivations and objectives for this project, that inspired the writing of this dissertation, are presented. Also, there is a brief description of the contents of each chapter.

1.1 Overview

Communication is the act of transmitting information from one point (sender) to another (receiver). To communicate has always been, since the beginning of time, a human need in order to approach distant communities. Long before this technological revolution we live in these days, smoke signals, drums, carrier-pigeons, just to name a few, were the options available to establish long distance communications.

Telecommunications truly began in 1844, when Samuel Morse transmitted the first message between Washington and Baltimore (Morse code). Telegraph, as shown in Figure 1.1, was the only means of communication for more than 30 years. Even after the invention of radio transmission, it remained in use for its intelligibility, even in the presence of noise and low signal intensity [telegraph-history.org, 2012].

Figure 1.1 – Samuel Morse and his telegraph
Source: [telegraph-history.org, 2012]

In 1876 a new fact would revolutionize telecommunications; it was the invention of the telephone, by Alexander Graham Bell. When ten years later came the carbon microphone (1886), the operational principles of telephone transmission were implemented, which prevailed until almost 1950s on all phones.

Also in 1886, Heinrich Hertz proved experimentally the analogy between electric and light waves.

Later on, Gugliermo Marconi, using the fundamentals of James Maxwell and Hertz, built the first radio transmitter in 1895 (Figure 1.2).

Figure 1.2 – Marconi and his radio transmitter

Source: [astrosurf.com, 2012]

In 1957, Sputnik, the first artificial satellite, was launched. On June 10, 1962 the first active communications satellite was put into orbit – Telstar – allowing transmission of telephone conversations, telephoto and colour television signals. It was the era of open telecommunications satellite.

The first mobile communications systems, called 1st Generation (1G) analogue systems, appeared in order to provide mobility to voice services. However, it was a quite limited system in terms of technology and quality of coverage.

Figure 1.3 – 1st Generation mobile phone

Source: [businessinsider.com, 2012]

The growing demand for mobile communications, associated with consequent technological developments, led to the emergence of a wide range of new services. Therefore, 2nd Generation (2G) was born, which provided advanced voice and data services, compatible with the Integrated Services Digital Network (ISDN). In Europe the system adopted was the Global System for Mobile communications (GSM), a highly successful standard.

The rise of the 3rd Generation (3G), called Universal Mobile Telecommunication System (UMTS) offered mobility and greater ability to integrate services such as voice, data, images and videos with high transmission rates.

The need to increase levels of efficiency and quality in communication networks has been growing exponentially in order to support different applications and services benefiting their users. Thus, the conditions to the appearance of Long Term Evolution (LTE) and, more recently, LTE-Advanced (LTE-A) were gathered, and the 4th Generation (4G) was born.

In order that each user can get the most from these technologies, and aiming to meet the expectations of an ever increasing and demanding market, it is necessary to resort to the use of planning techniques that promote the optimization and improvement of coverage and/or capacity. Thus, before the physical implementation of a mobile network it is necessary to analyse the coverage areas and make channel estimation through reliable tools and simulating the real environment, as realistic as possible.

1.2 Motivation, objectives and contributions

Routes used by commercial air traffic cover great part of the globe, with higher incidence in the most populated areas. The main objective of this project is to prove that it would be possible to have a global coverage network or, at least, a network able to fulfil the needs of users located in the most populated regions, where air traffic is denser, if LTE antennas (considering some modifications in this technology, *e.g.* signal processing, gains of the equipment, and also considering LTE-A) were installed in commercial aircrafts.

Users would be able to communicate to any part of the world; the nearest aircraft gets the signal and, since they are organized as a mesh network, it travels from aircraft to aircraft until reaching its final destination.

LTE was chosen to be implemented in this project because it is a recent technology and has the advantage of being compatible with existing resources in the High Speed Packet Access (HSPA) and GSM networks, enabling mobile operators to make a seamlessly transition to LTE. This represents a major evolution towards an all-IP (Internet Protocol) wireless network scenario, which provides mobile broadband capabilities and also enables the enhancement of the existing services and the introduction of new multimedia services.

This represents a breakthrough in terms of evolution of communications and also in terms of economy. With this solution, it is possible to cover great part of the planet using existing resources (the network is already built). When compared to solutions like satellites or

High Altitude Platforms, where it is necessary to build a network from the scratch and all the equipment involved in the eNode-B (eNB), plus the launching costs, one can easily conclude that this approach is much more profitable.

A new propagation model was deduced; the conditions in which the signal travels are quite different from what is verified in other cases. When the signal is travelling from aircraft to aircraft or it has line-of-sight (LoS) with the user equipment (UE), it can be considered that the signal suffers free space path loss because there are no obstacles on the way; however, when the aircraft is communicating to its final destination, or to the terrestrial network, it is necessary to consider the different scenarios and, consequently, the different attenuation caused by the obstacles that can be found in each of these environments, whether it is a rural, urban or suburban scenario.

This idea has been awarded with a Masterclass lectured by Michael O'Leary in the I Innovation Convention in Brussels, organized by the European Commission, for being one of the four most innovative ideas in Europe, in December 2011.

Later, in May 2012 we were invited to participate in a Portuguese TV program about innovative ideas and scientific projects called The Next Big Idea.

1.3 Dissertation structure

This dissertation comprises 5 chapters and 4 annexes. This chapter comes as an introduction to the following ones, contextualizing the reader. In chapter 2 a brief description of LTE, LTE-A and their similarities and differences is made; also in this chapter there is a glimpse about LTE network in terms of architecture and operation. Chapter 3 comprises the relevant commercial aviation concepts and particularities regarding this project. Chapter 4 gathers the results obtained considering propagation in free space and with obstacles in different environments, with the help of a propagation model deduced for this purpose. Finally, in chapter 5, some reflections are made in form of conclusions and future work is suggested. The last part of this document consists on the annexes, which provide auxiliary information, and the bibliography, where the references throughout the dissertation can be found.

Chapter 2

State of the Art

Throughout this chapter LTE and LTE-A are presented with the respective details that distinguish them, and a brief glimpse is made at the LTE network.

2.1 Introduction

The amount of traffic in mobile networks has grown immensely in the last years. Figure 2.1 stands out this growing trend for the next years. It is expected that mobile data traffic increases to 49 Exabytes per month by 2021, which constitutes 7 times more traffic than in 2016.

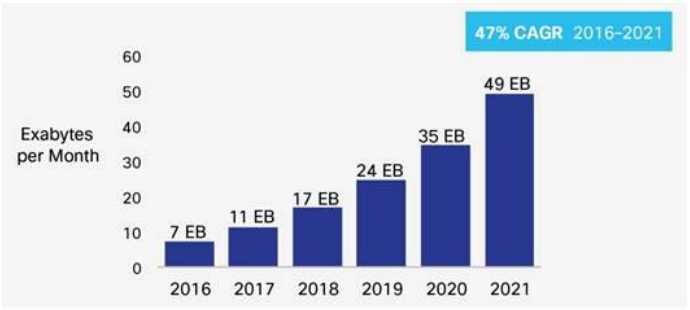

Figure 2.1 – Cisco forecasts 49 Exabytes per month of mobile data traffic by 2021 Source: [cisco.com, 2018]

Almost half of the global mobile traffic by 2021 will come from Asia Pacific (47%), the largest share when compared with the other regions presented. It is interesting to observe that North America will be surpassed by Central and Eastern Europe and Middle East and Africa, having the fourth-largest share in 2021, when it had the second largest share in 2016, as shown in Figure 2.2.

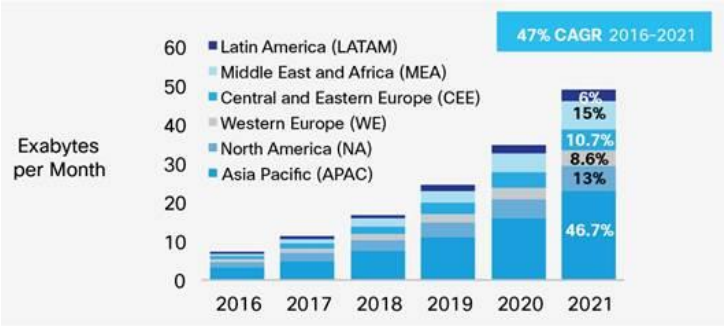

Figure 2.2 – Global mobile data traffic forecast by region
Source: [cisco.com, 2018]

This growth is due not only to a society that demands to be connected 24/7, but also due to the proliferation of high-end handsets, tablets and laptops. On mobile networks this

constitutes a major generator of traffic, since these devices may offer their users contents and applications not supported by previous generations of mobile devices.

Thus, at the same time, it was necessary for networks and standards to evolve, so those conditions could be satisfied. LTE appeared exactly to satisfy the increasingly demanding broadband society.

2.2 LTE Technologies

LTE operates in a more efficient fashion regarding the use of spectrum, at the same time providing much higher data rates than previous generations. That is because of the new technologies that came along with LTE, comparing to the previous cellular systems.

2.2.1 OFDM

The Orthogonal Frequency Division Multiplexing (OFDM) is based on the Frequency Division Multiplexing (FDM) technique; however, it is implemented with a digital modulation scheme. In FDM information sequences are mapped onto channels with parallel frequencies, separated by a guard interval in order to reduce interference between adjacent channels.

OFDM differs from traditional FDM because it contains several sub-carriers, orthogonal to each other, which carry the information sequences. To avoid the delay spread of the channel, a guard time is added to each OFDM symbol.

Figure 2.3 depicts an OFDM signal both in time and frequency domain.

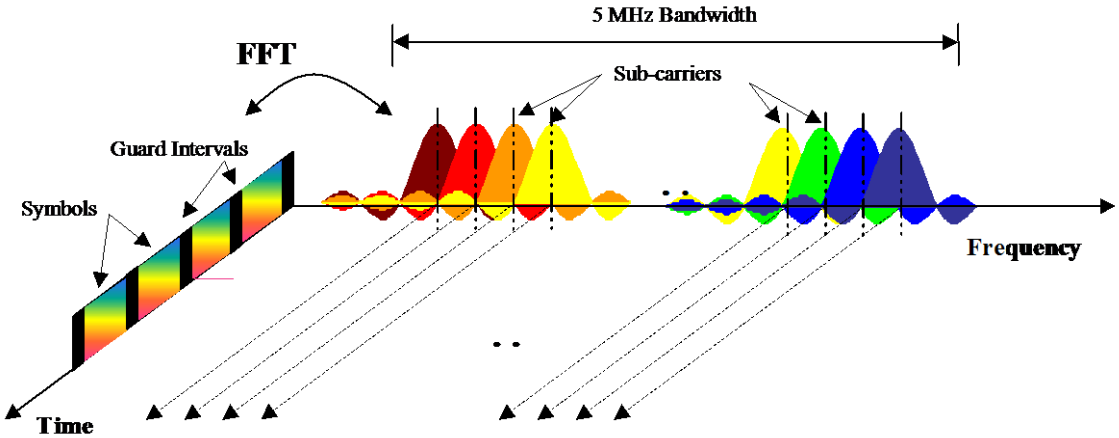

Figure 2.3 – Frequency-time representation of an OFDM signal

Source: [Rohde & Schwarz, 2012]

As previously mentioned, the guard interval is added after the OFDM symbol (T_u) in order to avoid the delay spread of the channel, reducing the interference between OFDM symbols. The range of this guard time T_g (corresponding to a prefix of N_p samples) shall be enough to cover the influence of the delay spread of the radio impulse response, allowing the performance of soft-handover.

The prefix is generated using the last block of the N_p samples of the OFDM symbol. Since the operation of inserting the prefix is a cyclic extension of the OFDM symbol, it is commonly referred to as Cyclic Prefix (*CP*). The representation of an OFDM symbol with the respective *CP* is in Figure 2.4.

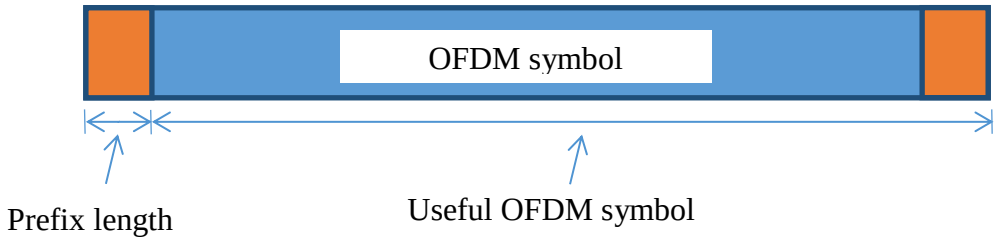

Figure 2.4 – OFDM symbol with *CP*

After inserting this guard time, the duration of the OFDM symbol, T_s, becomes:

$$T_s = T_u + T_g \tag{2.1}$$

Thereby having the sampling frequency and spacing between sub-carriers respectively:

$$F_0 = \frac{N + N_p}{T_s} \tag{2.2}$$

$$\Delta f = \frac{F_0}{N} \tag{2.3}$$

The cyclic prefix must absorb the energy of the scattered signal throughout the multipath channel. If the prefix is greater than the total delay spread of the channel, all the energy resulting from the interference between OFDM symbols is contained in the prefix. That is, if τ represents the total delay spread of the channel, we have:

$$T_g > \tau \tag{2.4}$$

The mapping of the modulated symbols on multiple sub-carriers allows an increase of the symbol duration. As the throughput on each sub-carrier is very low, the symbol duration obtained through OFDM is much higher when compared to single carrier modulation and similar total transmission bandwidth. In general, when the scattering of the propagation delay in the channel exceeds the guard time, the energy contained in the Inter-Symbol Interference (ISI) will be much smaller compared to the energy of the useful OFDM symbol. This happens while the symbol duration is much greater than the spread of the channel propagation delay, *i.e.*:

$$T_s \gg \tau \tag{2.5}$$

Although it is intended to get a great length of the OFDM symbol, in order to fight the spread in time, this factor may affect the ability to fight fast fading introducing loss in orthogonality between sub-carriers. Thus, the symbol duration shall remain lower than the minimum channel coherence. Since this time is inversely proportional to the maximum Doppler shift f_d, symbol duration T_s shall be chosen such that:

$$T_s \ll \frac{1}{f_d} \tag{2.6}$$

Due to the time-frequency duality, some arguments in the time domain can be easily converted to the frequency domain. The high number of OFDM sub-carriers makes the bandwidth of each individual sub-carrier small in relation to the total bandwidth of the signal. With the right number of sub-carriers, spacing between is inversely proportional to the scattering of the propagation delay in the channel τ, spacing between sub-carriers is described by:

$$\Delta f \ll \frac{1}{\tau} \tag{2.7}$$

In this case, fading in each sub-carrier is linear in frequency and can be modulated as a constant gain in the channel. The individual reception of modulated symbols transmitted in each sub-carrier is simplified if the channel contains linear fading, allowing the introduction of advanced Multiple Input Multiple Output (MIMO) schemes.

In order to combat the Doppler Effect, spacing between sub-carriers must be greater than the maximum Doppler shift f_d:

$$\Delta f \gg f_d \tag{2.8}$$

OFDM is considered a digital modulation technique that can be combined with multiple access (OFDMA). Multiple users can be multiplexed in time and frequency domain, with information from pilots and signalling. In the frequency domain (*i.e.* sub-carriers) the symbols of user data can be multiplexed into different numbers of useful sub-carriers. As such, sub-carriers (or groups of them), can be reserved for transmission of pilot information, signalling or other symbols. In the time domain it is possible to have multiplexing if it occurs at OFDM symbol rate or a multiple of it.

OFDM technology allows high data bandwidths to be transmitted in an efficient way, at the same time providing a high degree of resilience to reflections and interference. There are two different access schemes considered in LTE, one for uplink and the other for downlink – Single Carrier-FDMA (SC-FDMA) and OFDMA, respectively. It is necessary to have different technologies in uplink and downlink because of the different requirements between the two directions and the equipment at either end.

The choice of bandwidth is also one of the key parameters associated with the use of OFDM within LTE. This has particular influence in the number of carriers that can be accommodated in the OFDM signal and, consequently, in the symbol length and so forth.

LTE has defined a certain number of channel bandwidths. They are:

- 1,4 MHz;
- 3 MHz;
- 5MHz;
- 10 MHz;
- 15 MHz;
- 20 MHz.

It is important to mention that subcarriers are spaced 15 kHz apart from each other, which means that, being the symbol rate given by Equation 2.9, symbol rate is 66,7 μs.

$$T_{s[s]} = \frac{1}{f_{s[Hz]}} \tag{2.9}$$

Thus, in OFDM a large number of closed spaced carriers are modulated with low data rate. These signals do not interfere with each other, since they are orthogonal to each other and this prevents mutual interference. Orthogonality is achieved having the carrier spacing equal to the reciprocal of the symbol period, meaning that once the signals are demodulated they will have a whole number of cycles in the symbol period and their contribution will sum to zero.

Since all data to be transmitted is split across all the carriers, if some of these carriers are lost that will not constitute a problem because this way data can still be reconstructed.

The transmission scheme in the downlink is based on the conventional OFDM using *CP*, with constant sub-carrier spacing Δf = 15 kHz and a duration of *CP* that can be approximately 4.7 μs (5.2 μs if it is the first symbol) or approximately 16.7 μs, whether if it is being used normal or extended *CP*, respectively [Rohde & Schwarz, 2012].

Subcarriers are split into resource blocks in the downlink. This is advantageous considering that this way the system may allocate the data in a standard number of subcarriers. Resource blocks include 12 subcarriers, despite the signal bandwidth, and different signal bandwidths will have different number of resource blocks, as listed in Table 2.1 and slot structure can be seen in Figure 2.5.

It is possible to choose from three types of modulation within the OFDM signal:

1. QPSK;
2. 16QAM;
3. 64QAM.

This choice depends on the prevailing conditions. Lower orders of modulation like QPSK do not require much large signal to noise ratio, however it is not able to send data as fast as modulations with higher orders. These can only be used when there is sufficient signal to noise ratio, as will be confirmed in Chapter 4.

Channel bandwidth [MHz]	**Number of resource blocks**
1.4	6
3	15
5	25
10	50
15	75
20	100

Table 2.1 – Channel bandwidths and respective number of resource blocks

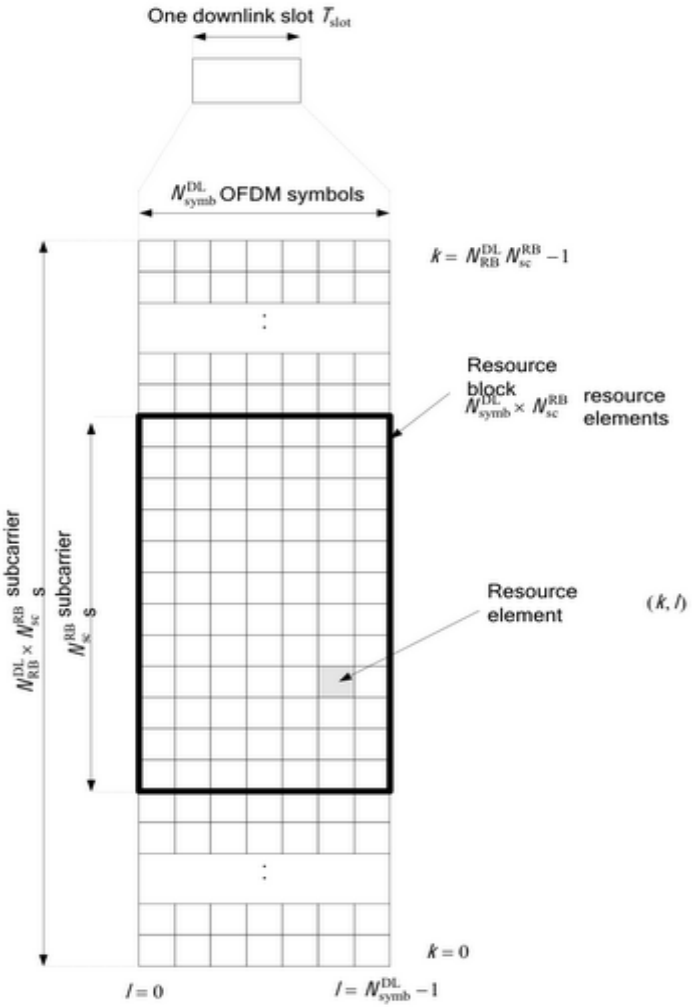

Figure 2.5 – Downlink resource grid

Source: [3gpplte-longtermevolution.blogspot.pt, 2012]

As previously mentioned, in the uplink a different concept is used – the SC-FDMA. This technique has the same complexity and performance that OFDMA using single carrier modulation and frequency domain equalization. Due to its single carrier structure, it has low Peak-to-Average Power Ratio (PAPR) being a huge advantage over OFDMA in the uplink, benefiting the efficiency of transmitting power from the handset.

The transmission with single carrier is used in the uplink with *CP*, in order to achieve orthogonality among users and allow efficient equalization in the receiver in the frequency domain.

In the uplink it is used the same generic frame structure as in the downlink. It also uses the same subcarrier spacing of 15 kHz and resource blocks width. The uplink modulation parameters are identical to the downlink parameters – including normal and extended *CP* length.

However, there is a difference when it comes to the subcarrier modulation. In the uplink, data is mapped onto a signal constellation that can be QPSK, 16QAM or 64QAM, depending on channel quality. Instead of using the QPSK or QAM symbols to modulate subcarriers directly, like is the case of OFDM, symbols in the uplink are sequentially fed into a serial/parallel converter and then into an PAPR. Thus, the result at the output of the Fast Fourier Transform (FFT) block is a discrete frequency domain representation of the QPSK/QAM symbol sequence. Before being converted back into time domain (Inverse Fast Fourier Transform - IFFT), the discrete Fourier terms at the output of the FFT block are mapped to subcarriers. Finally, a CP is appended and it is ready for transmission. Figure 2.6 illustrates the differences between OFDMA and SC-FDMA.

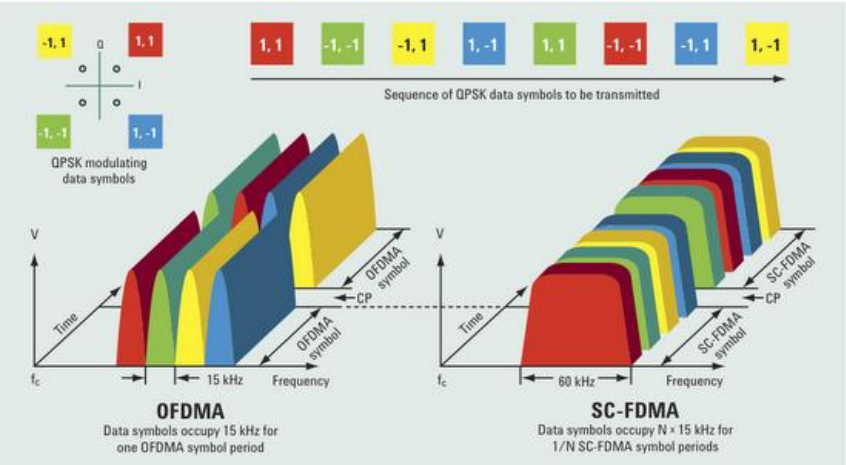

Figure 2.6 – OFDMA and SC-FDMA conceptual differences

Source: [3gpplte-longtermevolution.blogspot.pt, 2012]

2.2.2 TDD and FDD

Time Division Duplex (TDD) and Frequency Division Duplex (FDD) are two different standards of LTE. In FDD spectrum two pair bands are required, one for uplink and another for downlink, whereas in TDD only a single band is required since uplink and downlink are on the same frequency, separated in time. Both concepts are depicted in Figure 2.7.

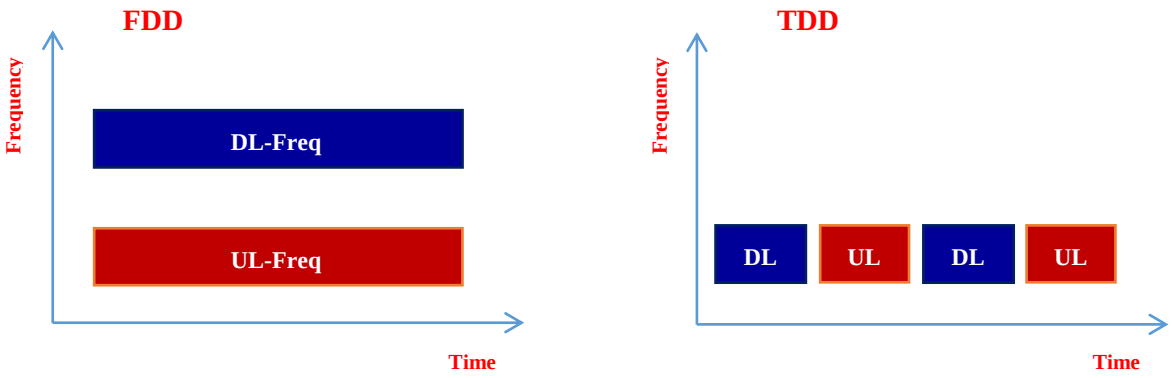

UL – Uplink

DL – Downlink

Figure 2.7 – FDD and TDD difference in LTE

Because of this conceptual difference, there are different LTE band allocations for TDD and FDD. However, band overlapping may occur, which means that despite its improbability, FDD and TDD can be both present on a particular LTE frequency band.

The most likely scenario is having a UE that will need to detect whether a TDD or FDD transmission shall be made on a particular band. Both TDD and FDD can be encountered by UEs, so there is the need for it to detect which type of transmission is currently being made in its current location and on that band.

Paired frequencies in FDD mode permit simultaneous transmission on two frequencies. The bands have enough separation so that transmitted signals do not impair the receiver performance, *i.e.*, too close signals may block and impair the sensitivity of the receiver.

LTE frequency bands are allocated numbers, therefore, from band 1 to band 25 frequencies are for paired spectrum, FDD, and bands from 33 to 43 are for unpaired spectrum, TDD, as shown in Tables A.1 and A.2 respectively, in Annex A.

2.2.3 MIMO

Along with OFDM, MIMO is a very important and innovative technology used in LTE to improve the performance of the system. Despite the complexity it introduces to the system, MIMO has the ability to further improve data throughput and spectral efficiency, above that achieved by using OFDM.

MIMO takes advantage of the multipath signal propagation and, rather than providing interference, these paths can be used in an advantageous way, by employing multiple antennas.

Once again, there are differences between methodologies in uplink and downlink. In the downlink there is a configuration of two transmit antennas at the BS and two receive antennas on the mobile terminal, however configurations with four antennas are also being considered. In the uplink the scheme will be different to take into account terminal complexity issues. Multiple User-MIMO (MU-MIMO) can be used, which means that multiple users can transmit at the same time on the same resource block. This is also referred to as Spatial Division Multiple Access (SDMA), requiring only one transmit antenna in the UE. In order to maintain the UE cost low, whilst taking advantage of the benefit of two or more transmit antennas, it can be used what is called transmit antenna selection. There are two transmit antennas in the UE, but only one transmit chain and amplifier. Also, there is a switch that will decide which of the antennas provide the best channel to the eNB, according to feedback provided by the eNB itself.

2.3 LTE-Advanced

It is not uncommon hearing or reading about LTE being called the 4th Generation (4G). This is not true, because LTE does not satisfy all the requirements to be designated like that. Instead, LTE is called 3,9G. The truly 4G is LTE-Advanced, the natural successor of LTE, having LTE as a starting point paired with some technologies that allow it to have a performance able to fulfil the requirements from 3GPP.

The differences between LTE and LTE-A in terms of system performance are listed in Table 2.2.

	LTE	**LTE-A**
Maximum downlink speed [bps]	100M	1G
Maximum uplink speed [bps]	50M	500M
Latency round trip time approximately [ms]	~10 ms	Less than 5 ms
3GPP releases	Rel 8	Rel 10
Access methodology	OFDMA/SC-FDMA	OFDMA/SC-FDMA

Table 2.2 – LTE and LTE-A differences in system performance

Adapted from [radio-electronics.com, 2012]

To achieve these LTE-A requirements related to system performance, some physical-layer enhancements have been introduced, such as carrier aggregation, enhanced downlink spatial multiplexing, uplink spatial multiplexing and support for heterogeneous networks [Ghosh *et al.*, 2010].

Carrier aggregation consists in aggregating multiple carriers, thus providing bandwidth extension up to 100 MHz [Iwamura *et al.*, 2010], whereas LTE supports channel bandwidths up to 20 MHz.

This significantly increases peak data rates (1 Gbps in the downlink and 500 Mbps in the uplink) and allows efficient interference management. In order to increase the spectral efficiency of the system, carrier aggregation also allows multi-carrier scheduling, carrier load balancing, quality-of-service (QoS) differentiation, interference coordination and heterogeneous deployment [Ghosh *et al.*, 2011]. Having QoS differentiation it is possible to create different subscription classes, so users have the possibility to assign a bandwidth and a preferred carrier based on their level of service agreement. Multi-carrier scheduling allows achieving improved throughput, since users can be scheduled in a carrier that is experiencing less interference. Inter-cell interference coordination techniques can be used with carrier aggregation to make sure that users are scheduled so that will generate less interference with surrounding cells. This is particularly interesting in a heterogeneous deployment supporting different power level cells and coverage areas. For instance, with soft reuse of the carriers, different carriers can be allocated to different coverage areas.

Carrier aggregation can be contiguous or non-contiguous, as the name implies, if carriers are contiguous or not. These concepts are depicted in Figure 2.8, where can also be seen the difference between the maximum bandwidth available in LTE (20 MHz) and in LTE-A (100MHz).

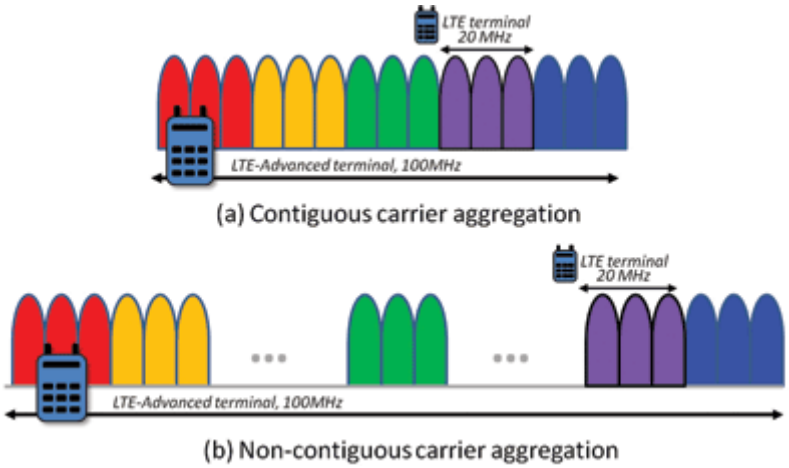

Figure 2.8 – Contiguous and non-contiguous carrier aggregation

Source: [electronicproducts.com, 2012]

Along with carrier aggregation, there is another technology worth mentioning, which is coordinated multipoint (CoMP). It consists on a range of different techniques that permit the dynamic coordination of transmission and reception over a variety of different base stations. The objective is to improve overall quality for the user whilst the utilisation of the network is being improved.

Even though it consists on a complex set of techniques, there are many advantages not only to the user, but also to the network operator. Providing connections to several base stations at the same time, data can go through least loaded base stations, providing a better resource utilisation. Reception performance is enhanced because of the use of several cell sites for each connection and the number of dropped calls should reduce. The overall received power at the handset tends to increase due to the joint reception from multiple base stations or sites. Also, it is possible to utilise the interference constructively, reducing the levels of interference.

As previously mentioned, CoMP consists on a group of techniques put together to enhance the overall system performance, using the resources more effectively and improve the end user service quality.

One of the most important parameters in LTE-A is the high data rates achievable. But as will be seen in Chapter 4 of this dissertation, high data rates are easy to maintain when the user is close to the base station, but the more the distance increases, the more difficult it is to maintain those high data rates. Particularly when it comes to the cell edges of the cell, the signal has its lowest strength (because of the distance from the eNB), and also interference levels from neighbouring eNBs presumably tend to be higher as the UE is closer to them.

Geographically separated eNBs dynamically coordinate to provide joint scheduling and transmissions as proving joint processing of the received signals. Thus, a UE at the edge of a cell can be served by two or more eNBs improving signals reception or transmission and increasing throughput. Figure 2.9 depicts the concept of CoMP.

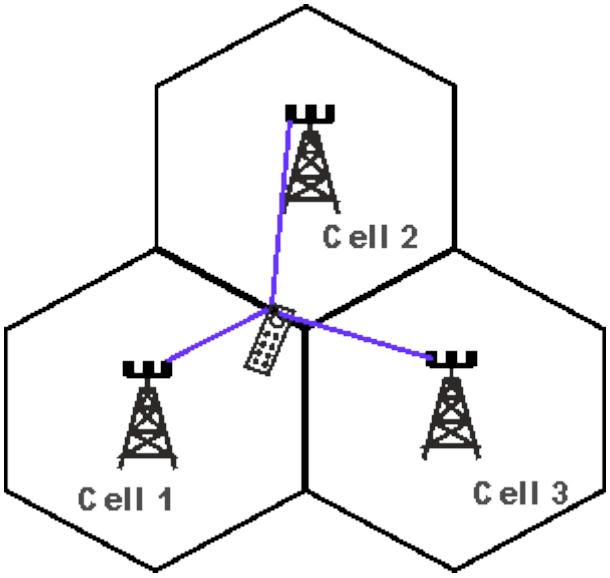

Figure 2.9 – LTE-A coordinated multipoint
Source: [radio-electronics.com, 2012]

2.4 LTE Network

2.4.1 Architecture

Contrarily to the previous cellular systems that supported circuit-switched services, LTE was designed to support only packet-switched services. UEs and Packet Data Network (PDN) are intended to be connected via Internet Protocol (IP). LTE encompasses the evolution of the radio access through the Evolved-UTRAN (E-UTRAN), along with an evolution of the non-radio aspects which is called System Architecture Evolution (SAE) including the Evolved Packet Core (EPC) network. Together, LTE and SAE comprise the Evolved Packet System (EPS).

In order to route IP traffic from a gateway in the PDN to the UE, EPS uses EPS bearers. A bearer is an IP packet flow with a defined QoS between the gateway and the UE. Together, E-UTRAN and EPC set up and release bearers as requested by applications [Sesia, *et.al*., 2009].

Figure 2.10 shows a representative scheme of the EPS network elements.

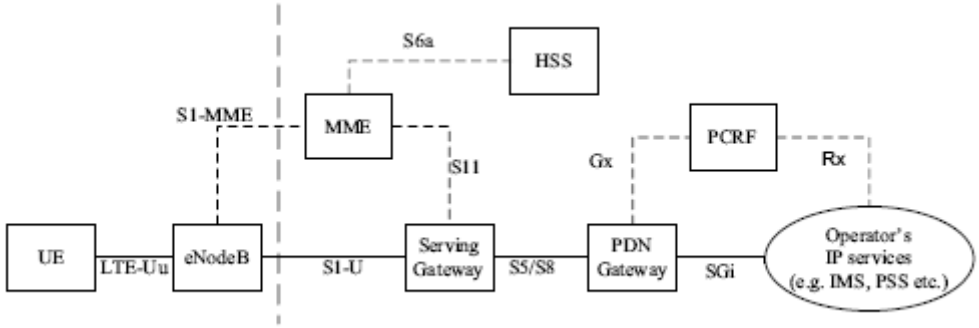

Figure 2.10 – The EPS network elements

Source: [Sesia *et.al*., 2009]

Despite all innovation in the network that brings major changes, SAE network is based upon GSM/WCDMA core networks, so that operations are simplified and the deployment is easy.

The Core Network (CN), which is called EPC in SAE, has the responsibility of the overall control of the UE and establishing the bearers. Its main logical nodes are:

- **PDN Gateway (P-GW):** it provides connectivity for the UE to external PDNs, being an entry and exit point for UE data. The UE may have connectivity with more than one P-GW in order to access multiple PDNs.
- **Serving Gateway (S-GW):** it is a data plane element with the objective to manage the user plane mobility and also works as the main border between the Radio Access Network (RAN) and the CN. S-GW maintains data paths between the eNBs and the P-GWs. Thus, S-GW constitutes an interface for the data PDN at the E-UTRAN. Moreover, S-GW serves as a mobility anchor when UEs move across areas served by different eNBs, ensuring the data path is maintained.
- **Mobility Management Entity (MME):** this is the main control node for the LTE SAE access network, having a number of features, such as bearer activation/de-activation or choice of S-GW for a UE, among others. This unit provides a considerable level of overall control functionality.

2.4.2 Self-Organized Networks

Microcells and femtocells are part of LTE deployment strategy, since smaller cell sizes are required in order to enable the greater levels of data traffic to be handled. Self-Organized Networks (SONs) appeared in this context, to manage the many more cells LTE implies as efficiently as possible.

SON has the following main elements:

- **Self-configuration:** The objective is to enable new BSs to become basically plug-and-play. The aim is for them to need as little manual intervention in the configuration process as possible. They are able to organize RF elements and also configure the backhaul.
- **Self-optimization:** Having the system set up, the BS (Base Station) has to be able to optimise the operational characteristics regarding the needs of the overall network.
- **Self-healing:** This is a major feature of LTE SON. By changing the characteristics of the network, the problem is masked until fixed. For instance, the boundaries of adjacent cells can be increased by changing antenna directions and increasing power levels, etc.

Chapter 3

Commercial Aviation

This chapter provides information about commercial aviation. Routes, airports distribution, traffic, rates of arrivals and departures in the busiest airports in the world, frequencies used in aircraft traffic control and some flight specifications, necessary to calculations done in this and next chapter, are analysed and discussed.

3.1 Introduction

Although its history goes back a little more than a century, aviation evolved in a fast pace, mainly due to its use in wars and its economic advantages.

During the First World War, the importance of aircraft was properly noticed and this gave a strong impetus to its development. The economic crisis felt after the war and the decreasing demand for military aircraft, has made the aviation industry seek for new challenges, turning towards the civil aviation market. Challenges have changed with the growth of this market sector. New milestones should be established, the trans-Atlantic and long duration flights were goals to be achieved, and the aircraft industry followed this trend [Crouch, 2004].

Civil aviation grew in Europe and United States. Advances in the science of aerodynamics, technical improvements in aircraft construction, equipment, controls and cockpits allowed aircrafts to fly at higher altitudes, faster and taking more cargo and passengers [Grant, 2002].

In the Second World War (1939-1945) aircrafts had a major role. Consequently, this led to a technological development so great that a lot of inventions appeared in a short period of time, such as jet aircraft, helicopter and electronic systems, among others [Crouch, 2004].

The early fifties brought the first jet aircrafts, but it was not until 1958 that the first passenger aircraft started to operate successfully, carrying new challenges for the aviation industry seeking bigger and faster aircrafts, whilst their systems became increasingly complex [Grant, 2002].

From the seventies came the supersonic aircraft and the first automatic navigation systems. In the eighties, electronic flight management systems appeared, and finally, in the nineties, digital systems were introduced.

Having said that, on one hand this chapter contextualizes the current aviation scenario justifying the importance of this project, in terms of potential number of users; on the other, the necessary data for calculations in subsequent chapters are provided. Matters such as worldwide routes, distribution of airports around the globe, the thirty busiest airports by international passenger traffic, as well as the flight specifications required for calculations made in this dissertation, are also present in this chapter.

3.2 Worldwide routes

Figure 3.1 depicts a map of scheduled airline traffic around the world. The green lines represent 54317 routes [wikipedia.org, 2011a].

As can be seen, the vast majority of routes are explored in the northern hemisphere, namely in Europe and United States. One possible explanation can be the fact that most part of the travellers fly from developed countries to other developed countries and most of them are located in the northern hemisphere.

Figure 3.1 – Worldwide airline traffic

Source: [wikipedia.org, 2011a]

Countries with more Internet access per capita [wikipedia.org, 2018b], as illustrated in Figure 3.2, would greatly benefit from this technology; since their airspace has more aircrafts, there would be a wider coverage, allowing for more people to use this new kind of network, while alleviating traffic in the existing terrestrial networks, thus avoiding congestion and improving their capacity.

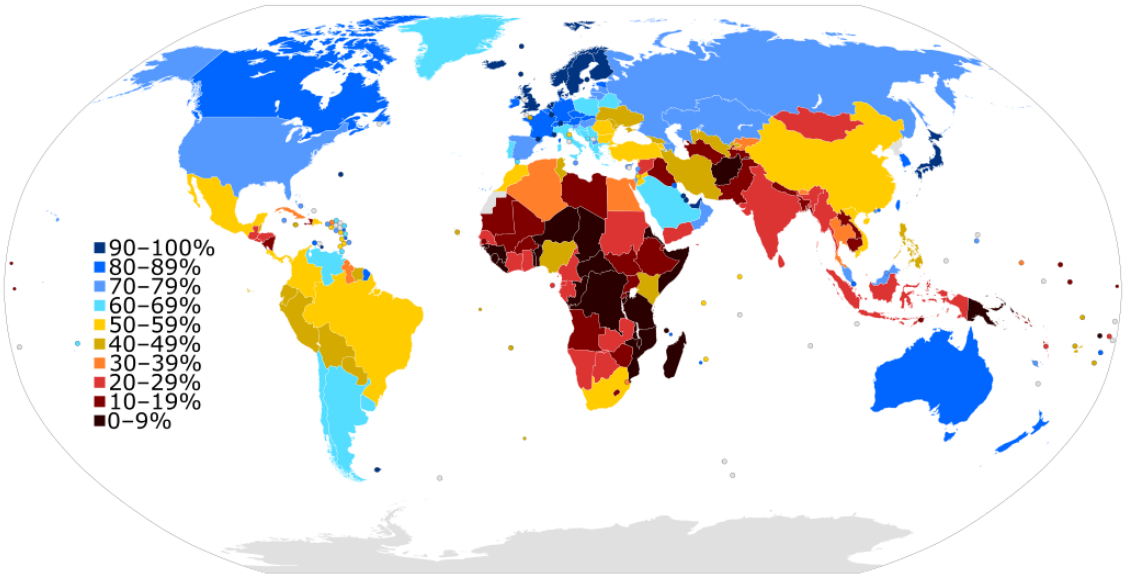

Figure 3.2 – Percentage of Internet users in 2015 per country according to its population
Source: [wikipedia.org, 2018a]

However, southern hemisphere would also benefit from this network, despite the fewer connections existing, once the number of users is smaller when compared to the ones existing in the northern hemisphere. It would be beneficial not only in terms of coverage; because implementation costs are not supposed to be high, neither should be its access cost, making this a means to those people most in need in the underdeveloped countries to have access to Internet.

If this becomes technically possible to implement, *i.e.*, a communications network supported on commercial aircrafts, it is of utmost importance and interest to take this step, because from users that would have at their disposal another means to communicate, to the existing networks that would have their traffic alleviated, the advantages are numerous and should be considered.

The map in Figure 3.3 presents the geographical distribution of airports around the world. There are over 10000 airports represented, each marked by a red dot [openflights.org, 2018]. In [openflights.org, 2018] a list of existing airlines and routes all over the world is also available to consult.

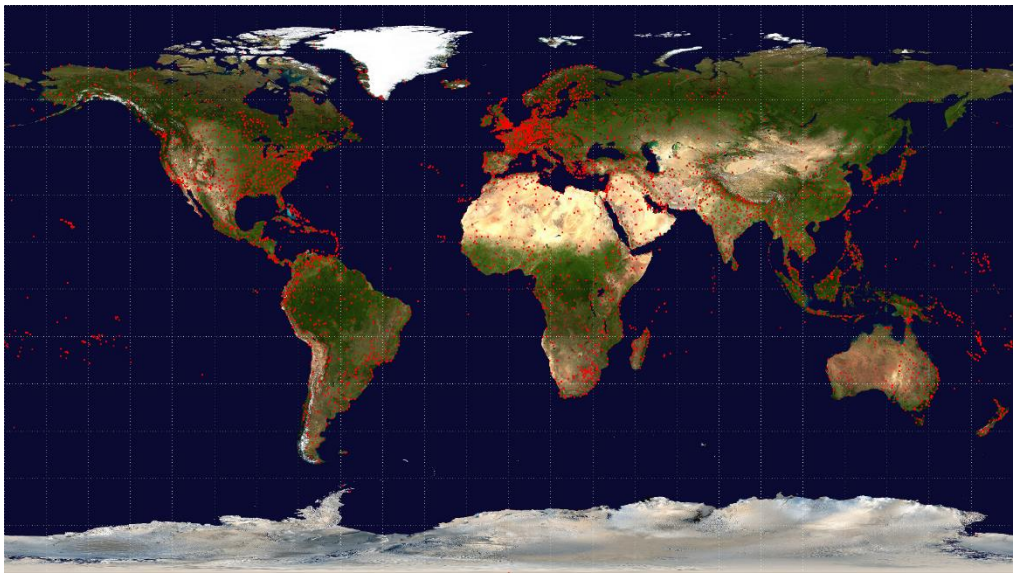

Figure 3.3 – Worldwide airports

Source: [openflights.org, 2018]

3.3 Generated traffic at major airports

Table B.1 lists the top twenty busiest airports in the world according to passenger traffic, during the year 2017. One passenger refers to someone who arrives in, departs from or transfers through a given airport on a given day. Lisbon Airport is not one of the busiest airports in the world, as can be seen by the values: in the year 2016, the number of total passengers was 22 449 289 [ana.pt, 2018].

Summing the number of passengers from all the twenty airports and then dividing that result by the 365 days of the year, it gives us the average number of passengers per day throughout the year, which are about four million people.

In Figure 3.4, as far as European network is concerned, it is shown that traffic increased about 2.8% in 2016 when compared to 2015, and this increasing trend is verified since 2013 [Eurocontrol, 2018].

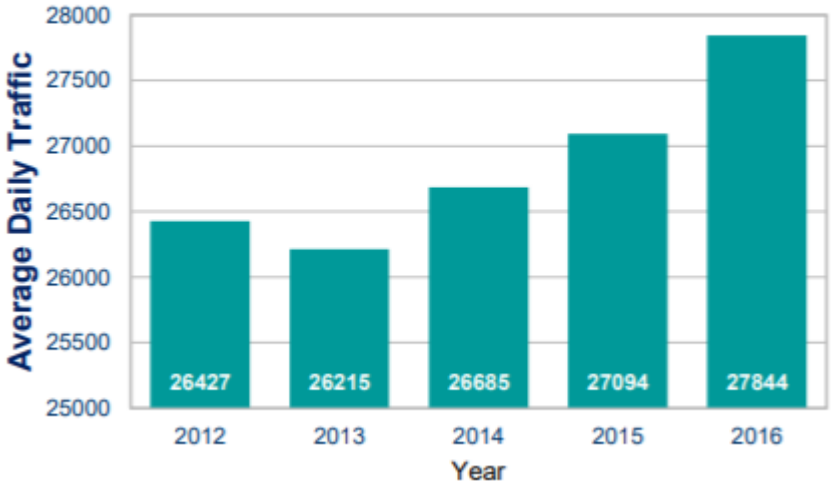

Figure 3.4 – Average daily traffic per year

Source: [Eurocontrol, 2018]

3.4 Commercial aircrafts flight specifications

As drivers on roadways have rules to follow and laws they must obey, there are also rules and laws to govern pilots flying in the airways. These rules are designed to prevent the chaos that would occur if everyone who piloted an aircraft flew without regard for others. Air traffic controllers use these laws as the basis for their operating rules and provide pilots flight following, traffic advisories and routing to avoid weather and maximize efficiency, since they have to manage all flights needing to use the same airspace, the same runways and same airports at about the same time.

There are several factors to take into account when considering the specifications of a given flight, such as the type of aircraft considered, weather conditions, velocity it can achieve, etc.

Weather conditions are crucial in aviation, since many factors of a flight depend on them. Speed can be taken as an example of this dependency on weather conditions, especially the wind, which can enhance or diminish the speed of an aircraft and, consequently, the time it takes to reach its destination. Because of this, two different speeds should be considered: ground speed and air speed. Ground speed refers to the speed at which the aircraft moves with respect to the ground. Air speed is the speed at which the aircraft moves in relation to the air.

As illustrated in Figure 3.5, when the air has no measurable wind (the aircraft is flying through still air), ground speed and air speed have the same value. When the aircraft moves

with the wind, the value of ground speed will be equal to the sum of both air speed and wind speed. In turn, when the aircraft flies against the wind, its ground speed is the difference between air speed and wind speed [virtualskies.arc.nasa.gov, 2011].

For this reason, with favourable winds, in a Lisbon – New York route, for instance, an hour can be spared.

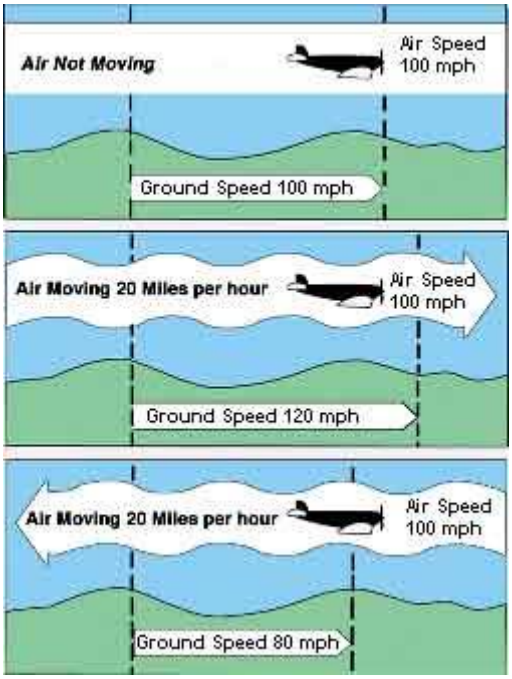

Figure 3.5 – Ground speed and air speed

Source: [virtualskies.arc.nasa.gov, 2011]

The time an aircraft takes to reach the cruising altitude is another factor that quite depends on weather conditions. But, generically, one can assume that most aircrafts can go up to about 600 metres per minute, which means that in approximately 20 minutes, and with an average angle ($\overline{\alpha}$) of about 3,5º, it can reach cruising altitude, that is approximately between 10000 and 12000 metres.

The lift-off speed varies from model to model of aircraft. In average it can be considered that when it is about to take-off, the aircraft reaches a speed of 270 km/h [aerospaceweb.org, 2018]. Some requirements concerning take-off velocity must be taken into account, as before the aircraft lifts, its speed must vary in accordance to some criteria. Figure 3.6 depicts the several velocities that must be observed along the runway.

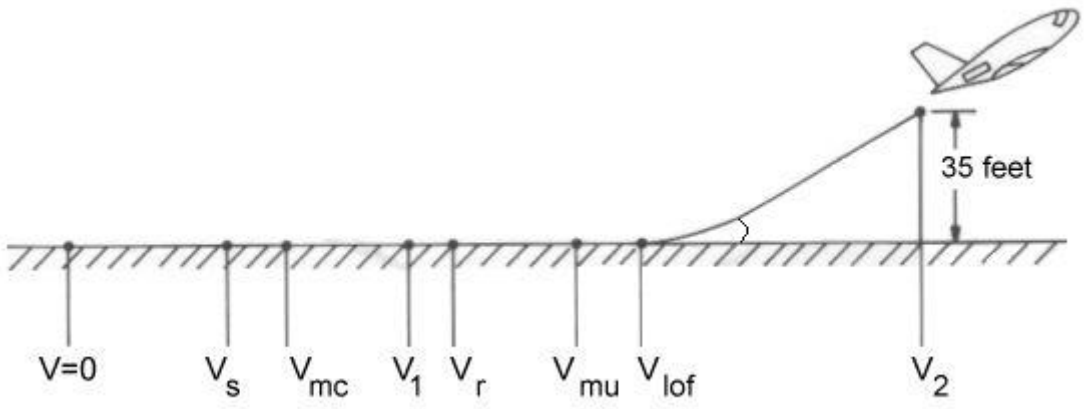

Figure 3.6 – Take-off velocities for a multiengine aircraft

Adapted from [aerospaceweb.org, 2018]

The aircraft starts in the position where $v = 0$, and then its speed increases until it reaches v_s (stall speed), which is the slowest speed at which the aircraft can travel and generate the sufficient lift to remain or to become airborne. Stall speed can be obtained through the lift equation:

$$L_{[N]} = \frac{1}{2} \cdot \rho \cdot v_s^{\,2} \cdot S_{ref} \cdot C_L \tag{3.1}$$

Knowing that it is necessary to have enough lift (L) to neutralize the take-off weight (W), knowing the reference area (S_{ref}), and the density of the take-off altitude (ρ), the most difficult value to estimate is the lift coefficient (C_L). However, a typical values are 2 to 2.5 for a traditional airliner. Having these values, stall speed comes as:

$$v_{s[m/s]} = \sqrt{\frac{2 \cdot W}{\rho \cdot S_{ref} \cdot C_L}} \tag{3.2}$$

An aircraft is capable of taking off when it reaches the stall speed; however, because this is a very unstable condition, and there is the hypothesis of the aircraft to drop back onto the runway, a number of additional speed requirements have been implemented.

The first one is the minimum control speed, v_{mc}, and it is related to multi-engine aircrafts. If an engine fails during the take-off run, usually a yawing moment is observed since the engine(s) on the other side of the aircraft produce more thrust. This causes the nose to turn side-to-side and is countered by a deflection of the rudder, producing a yaw moment in the opposite direction. This way, the two moments cancel each other and keep the aircraft headed straight down the runway. Below this minimum control speed there is not enough aerodynamic force generated by the rudder to produce the necessary correcting yaw.

The following speed, v_1, is also related to the failure of an engine during the take-off run. It is extremely important that if an engine fails far down the runway, the aircraft must have enough speed to continue the take-off in a safely manner, or, on the other hand, if it fails early in the take-off, there must be enough runway left to abort the take-off. This speed, v_1, comes up to help the pilot to decide whether to abort the take-off or not, in the event of engine failure. If the engine fails after v_1 has been exceeded, it should continue the take-off.

After v_1, the next velocity of interest is v_r, the rotation speed, and as the name indicates, it is the speed at which the aircraft can begin to rotate its nose into the air. This has to be at least 5% greater than v_{mc}.

The minimum unstick speed, v_{mu}, defines the point where the aircraft could take-off if its tail were to actually scrape the ground. However, this is impossible as it would damage the aircraft, so it actually lifts off at a slightly greater velocity, v_{lof}, the liftoff speed. This should be at least 10% greater than v_{mu} when all engines are operating and 5% greater when one engine has failed.

Finally, there is v_2, the take-off climb speed, which must be reached at an altitude high enough to clear a given obstacle. This height is defined as 10.7 metres. This speed must be at least 20% greater than stall speed, v_s, and 10% greater than v_{mc} [aerospaceweb.org, 2018]. Table 3.1 summarizes these speeds and their respective requirements.

Speed	Description	Requirement
v_s	Stall speed in take-off configuration	-
v_{mc}	Minimum control speed with OEI	-
v_1	OEI decision speed	= or > v_{mc}
v_r	Rotation speed	5% > v_{mc}
v_{mu}	Minimum unstick speed for safe flight	= or > v_s
v_{lof}	Liftoff speed	10% > v_{mu} 5% > v_{mu} (OEI)
v_2	Take-off climb speed at 10,7 m	20% > v_s 10% > v_{mc}

Table 3.1 – Take-off velocities and respective requirements

Source: [aerospaceweb.org, 2018]

Temperature and pressure are other influent factors to consider. However, a typical value for cruising speed, for instance, considering a Boeing 747-400 travelling at approximately 10 000 metres above the ground is about 913 km/h [boeing.com, 2018].

At Lisbon airport, and at peak traffic, time between arrivals and departures is approximately one minute. Air traffic controllers struggle to make this number as close to one as possible. Ideally, for all aircraft arriving with two minutes apart, they would be able to put another one taking off in the middle. This gives, in theory, 60 movements per hour. Obviously this is not feasible, and the best ever got was 52 movements per hour. But, as seen on Table B.1, there are airports much busier, and taking the London-Heathrow airport as an example, it has parallel lanes, in which one is used only for landings and another is for take-offs only. Under these conditions, the number of movements per hour increases substantially.

Considering that an aircraft is approaching an airport, a normal descent occurs at constant airspeed and also constant angle of descent [wikipedia.org, 2011b]. When an aircraft makes its final approach to land on a runway, the trajectory it describes is ideally a gentle downward slope, therefore this is called the approach slope. Commonly, an approach slope is 3º from the horizontal. Nevertheless, some airports may have different values for this angle, because of topography, buildings, etc. For example, London City airport has a 5.5º approach slope [wikipedia.org, 2011c].

When it comes to landing speed, once again, it depends on the model of aircraft in question. However, a typical value that can be considered is about 240 km/h [physicsforums.com, 2011]. Taking into account the standard approach slope, with 3º of angle, the vertical speed on a 240 km/h touchdown is about 13 km/h, given by:

$$v_{[Km/h]} = 240 \times \sin 3 \approx 13 \tag{3.3}$$

There is also an important issue to be considered and that is the distance between aircrafts when they are in the enroute scenario and also when they are approaching the terminal. Typically, when aircrafts are at the same altitude, they should be separated by about 9200 metres. Nearby the airport, if at the same altitude, this distance decreases to about 5500 metres [airliners.net, 2011].

3.5 Spectrum used in aircraft control communications

The main goal of all communications in aviation is to provide unambiguous, correct and current information to aircrews and controllers, contributing to the safety and reliability of air transportation.

Both pilot/co-pilot and air traffic controller play the role of sender and receiver when communicating. Radio communications follow the simplex system, which means that only one person can talk at a time, otherwise their simultaneous transmissions would block out each other's signal.

The radio spectrum used by aeronautical communications is shown in Figures 3.7 and 3.8. The VHF and HF communications band may be the ones that have more interest, however, future communications bands are likely to be stressed and become VHF (108 – 137 MHz), L band (960 – 1215 MHz), S band (2.7 – 3.1 GHz) and C band (5 – 5.250 GHz) or a hybrid of these [Stacey, 2008].

These figures also depict adjacent allocations to navigation and surveillance functions, as well as some not so well known allocations reserved to specialist services.

When it comes to communication, navigation and surveillance (CNS) functions, separate allocations have been made for aviation services as defined in ITU. Since the spectrum is a limited resource, there has been a growing interest towards sharing radio spectra between radio services. Also, there is an interest in CNS applications to share the same band. This kind of complicates the business of spectrum allocation, sharing and protection from harmful interference.

As far as civil aviation is concerned, the range of frequencies used to communicate is comprehended between 118 MHz and 137 MHz. In case of emergency the frequencies of 121.5 MHz or 243 MHz are used to get attention quickly [virtualskies.arc.nasa.gov, 2011].

Interference is perhaps the most important problem to avoid, as it can put at stake the safety of the flight, but since aircrafts use VHF to communicate and LTE uses different frequencies this is also a problem that can be easily overcome.

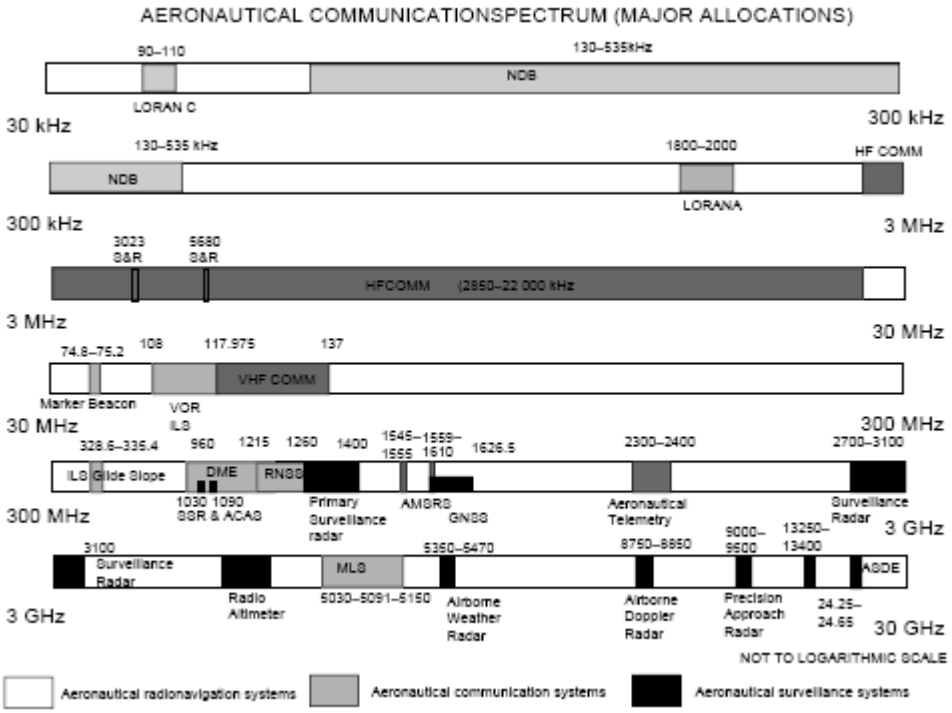

Figure 3.7 – Communications radio navigation and surveillance bands

Source: [Stacey, 2008]

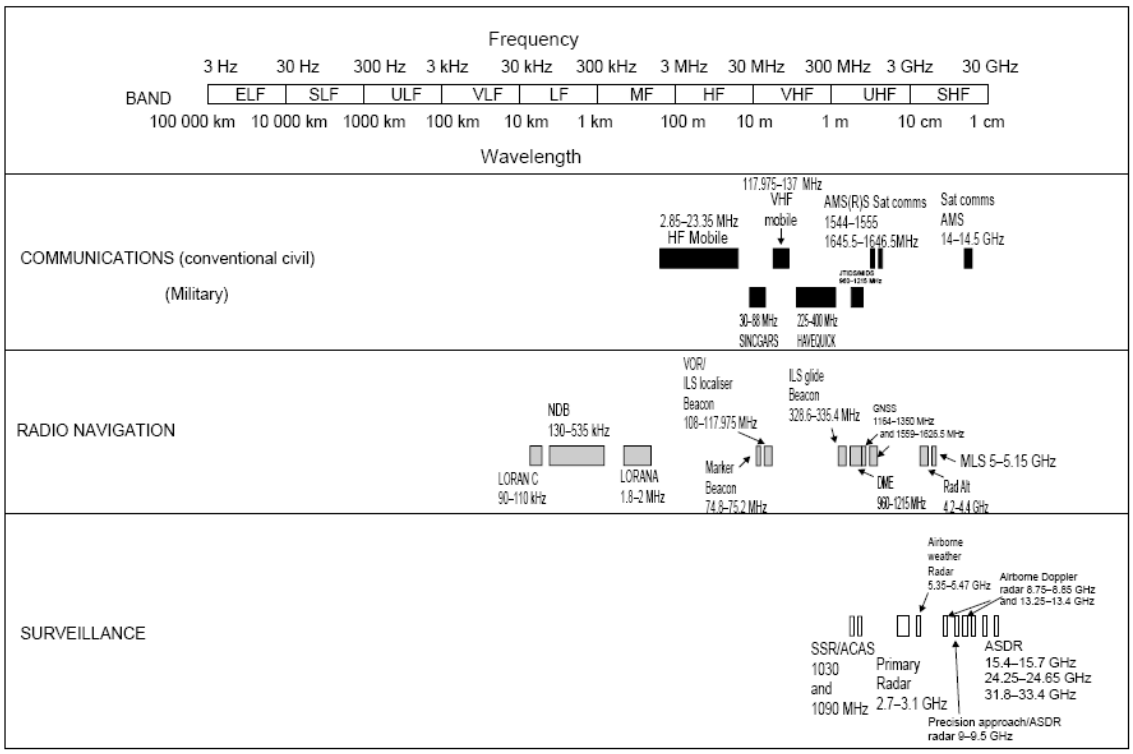

Figure 3.8 – Aeronautical radio spectrum

Source: [Stacey, 2008]

Chapter 4

Physical Layer

In this chapter, the theoretic performance of the project is analysed, according to LTE/LTE-Advanced standards specified by 3GPP. Also the results obtained are presented and discussed.

4.1 Introduction

According to [netseminar.stanford.edu, 2012], the power transmitted by a base station is approximately 43 dBm - considering a macro cells scenario, where conventional base stations are used, with dedicated backhaul and open to public access - and the antenna gain has a value that can be from around 12 to 15 dBi. For calculations purpose, the values considered were 43 dBm for the transmitted power and 13.5 dBi for the antenna gain (the middle value between 12 and 15 dBi).

Having these elements, it is possible to get the EIRP (Equivalent Isotropic Radiated Power), which value is approximately 56.5 dBm, given by:

$$EIRP_{[dBm]} = P_{t[dBm]} + G_{a[dBi]} \tag{4.1}$$

As far as the UE is concerned, according to [Sesia, *et al.*, 2009] the maximum output power is 23 dBm and this should be satisfied within a range of ±2 dB.

LTE frequency bands are allocated numbers. Regular additions to these LTE frequency bands/spectrum allocations are being made as an outcome of negotiations that take place at ITU (International Telecommunication Union) regulatory meetings. This results not only from the digital dividend, but also from the pressure that comes up from the fact the need for mobile communications is an ever growing phenomenon. A fact worth of concern is that the new LTE spectrum allocations are often 10-20 MHz bandwidth, which is quite small, and taking into account that LTE-Advanced needs 100 MHz bandwidths, it will be necessary to use channel aggregation over a wide set of frequencies.

In this dissertation FDD was the only considered. By the time the calculations were done, the list of frequencies was not complete as listed in Table A.1. The frequencies considered by that time are listed in Table 4.1. The fact that these recently added frequencies were not considered does not constitute a problem, since the values used for the most important calculations were the ones corresponding to the highest and lowest frequencies, and the recently added values are between these considered, therefore, they would not be considered anyway.

LTE Band Number	Uplink [MHz]		Downlink [MHz]	
1	1920	1980	2110	2170
2	1850	1910	1930	1990
3	1710	1785	1805	1880
4	1710	1755	2110	2155
5	824	849	869	894
6	830	840	875	885
7	2500	2570	2620	2690
8	880	915	925	960
9	1749.9	1784.9	1844.9	1879.9
10	1710	1770	2110	2170
11	1427.9	1452.9	1475.9	1500.9
12	698	716	728	746
13	777	787	746	756
14	788	798	758	768
15	1900	1920	2600	2620
16	2010	2025	2585	2600
17	704	716	734	746
18	815	830	860	875
19	830	845	875	890
20	832	862	791	821
21	1447.9	1462.9	1495.5	1510.9
22	3410	3500	3510	3600

Table 4.1 – FDD LTE bands and frequencies considered
(Adapted from [radio-electronics.com, 2012])

It has been decided to use the value in between the pairs of frequencies both for uplink and downlink for calculations purpose. The chosen frequencies are presented in Table 4.2.

Having the frequencies chosen, the next step was to calculate the free space attenuation and analyse its consequences in the power received by the UE. Afterwards it is necessary to take into account that one of the many constraints during an established communication is not only the free space path loss that affects the performance of the connection, but also the environment where the signal propagates.

f_{up} [MHz]	f_{down} [MHz]
1950	2140
1880	1960
1747.5	1842.5
1732.5	2132.5
836.5	881.5
835	880
2535	2655
897.5	942.5
1767.4	1862.4
1740	2140
1440.4	1488.4
707	737
782	751
793	763
1910	2610
2017.5	2592.5
710	740
822.5	867.5
837.5	882.5
847	806
1455.4	1503.2
3455	3555

Table 4.2 – Chosen frequencies for uplink and downlink

4.2 Radio Propagation Models

A primary concern when projecting a connection between two points should be the ratio between the transmitter output power and the power at the receiver input [Salema, 2002]. In this specific case, the ratio between the power at the terminals of the transmitter placed in the aircraft, and the power received by the UE.

Because nature imposes its constraints, the received power is always less than the transmitted power. There are considerable propagation loss factors, and despite these problems being well identified and known by scientists, it is not possible to calculate the exact value of its prejudice. Nevertheless, it is possible to find approximate values and tendencies, through radio propagation modelling.

Radio propagation models consist on empirical mathematical formulations used to characterize the propagation of a radio wave as a function of frequency, distance and other elements considered relevant.

It is of paramount importance that propagation models get as close to reality as possible, so they can be seen as reliable and helpful tools when it comes to planning a mobile communications network.

In the specific case of this project there are two possible situations:

✈ The signal travels in LoS, which can happen when the aircraft is communicating with another aircraft or when the user is communicating with an aircraft in LoS. In this case it was only considered free space attenuation according to the Friis model;

✈ There is no LoS, and in this case it had to be considered the attenuation the signal suffers, according to a propagation model deduced to this purpose.

4.2.1 Propagation in Free Space

In a first approach it was considered that between transmitter and receiver there is nothing but free space. In this case, where transmitter and receiver have a clear, unobstructed LoS path between them, it is used the free space propagation model to predict the damage in the received signal.

In 1946 Harald T. Friis published his analytic formula for transmission loss [wikipedia, 2012], which is still employed nowadays. This model relates the power transmitted from one antenna to the other, in ideal conditions, and can be represented by Equation 4.2:

$$\frac{P_r}{P_t} = G_t \cdot G_r \cdot \left(\frac{\lambda}{4\pi R} \right)^2 \tag{4.2}$$

where P_r is the received power, P_t is the transmitted power, G_r and G_t refer to the gain of the receiver and transmitter antennas, respectively, λ is the wavelength and R is the distance between antennas.

Most large-scale radio wave propagation models predict that received power decays as a function of the distance that separates transmitter and receiver raised to some power. Free space model is an example of this situation [Rappaport, 2002].

After analysing which values for the respective powers were on the line, it was calculated the free space path loss both for uplink and downlink. The distance considered between the aircraft and the UE was 12 km, because this is typically the highest altitude a commercial aircraft flies and, consequently, the worst case scenario for the signal to propagate

since the longer the distance, the higher the attenuation value. Equation 4.3 represents the free space model, where d is the distance between the antennas, λ is the wavelength and A_0 gives the value of the free space path loss.

$$A_{0[dB]} = 20 \cdot \log\left(\frac{4\pi d_{[m]}}{\lambda_{[m]}}\right) \tag{4.3}$$

Knowing the frequencies, the value of λ is obtained by:

$$\lambda_{[m]} = \frac{c_{[m/s]}}{f_{[Hz]}} \tag{4.4}$$

Where f is the frequency in use (whether it is downlink or uplink) and c is the value of the speed of light, which exact value is 299792458 [m/s].

Applying Equation 4.4 in Equation 4.3, another equation to calculate free space attenuation arises:

$$A_{0[dB]} = 32.4 + 20 \cdot \log_{10}(d_{[km]}) + 20 \cdot \log_{10}(f_{[MHz]}) \tag{4.5}$$

Values obtained with Equation 4.5 for free space attenuation are listed in Table C.1 according to the different frequencies, and for a maximum distance of 12 km between UE and aircraft. For a better understanding, Figures 4.1 and 4.2 illustrate the free space path loss observed in uplink and downlink, respectively.

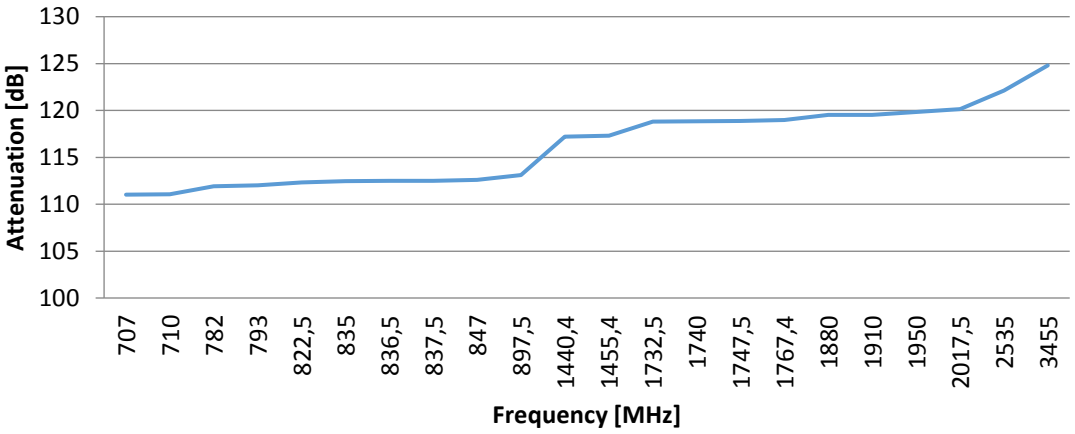

Figure 4.1 – Free space attenuation in the uplink

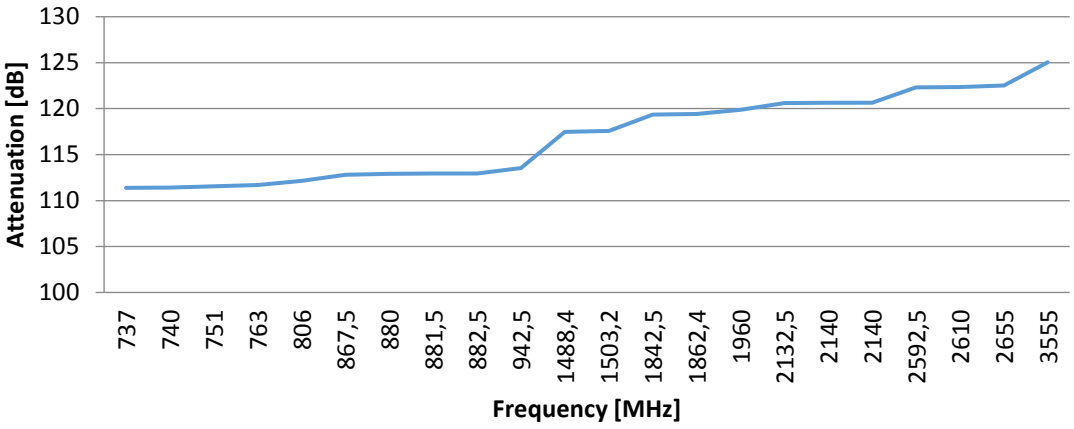

Figure 4.2 – Free space attenuation in the downlink

Both graphics have the same evolution, as expected. The higher the frequency, the higher the free space attenuation suffered by the signal.

Values for free space attenuation in the uplink vary from approximately 111.022 dB to 124.803 dB, corresponding to the lowest and highest frequency considered, respectively. As far as downlink is considered, values range from 111.383 dB to 125.050 dB, also corresponding to the lowest and highest frequency respectively. This results show that having the possibility to choose among several frequencies, the lower the frequency chosen, the less attenuation the signal will suffer. The slopes observed in the graphics are due to scale formatting.

Now that the values for free space path loss are known, it is time to ascertain the values for the power received by the UE, according to the corresponding frequencies, through Equation 4.6:

$$P_{r_{UE[dBm]}} = EIRP_{eNB[dBm]} - A_{0_{down[dB]}} \tag{4.6}$$

Where $EIRP_{eNB[dBm]}$ is the Equivalent Isotropic Radiated Power from the eNB, *i.e.*, the antenna placed in the aircraft and $A_{0down[dB]}$ is the free space attenuation obtained previously for the downlink. Figure 4.3 represents the power received by the UE according to the frequency used for the transmission. It is clearly noticeable that the higher the frequency, the lower the power received. Values oscillate between -54.184 dBm and -69.55 dBm. This is consequence of the previous analysis, where it was observed that the higher the frequency, the higher the attenuation. Because the received power depends directly on the attenuation, these values are the expected. Table C.2, in Annex C, lists the values obtained for the power received by the UE, both in dBm and in linear units.

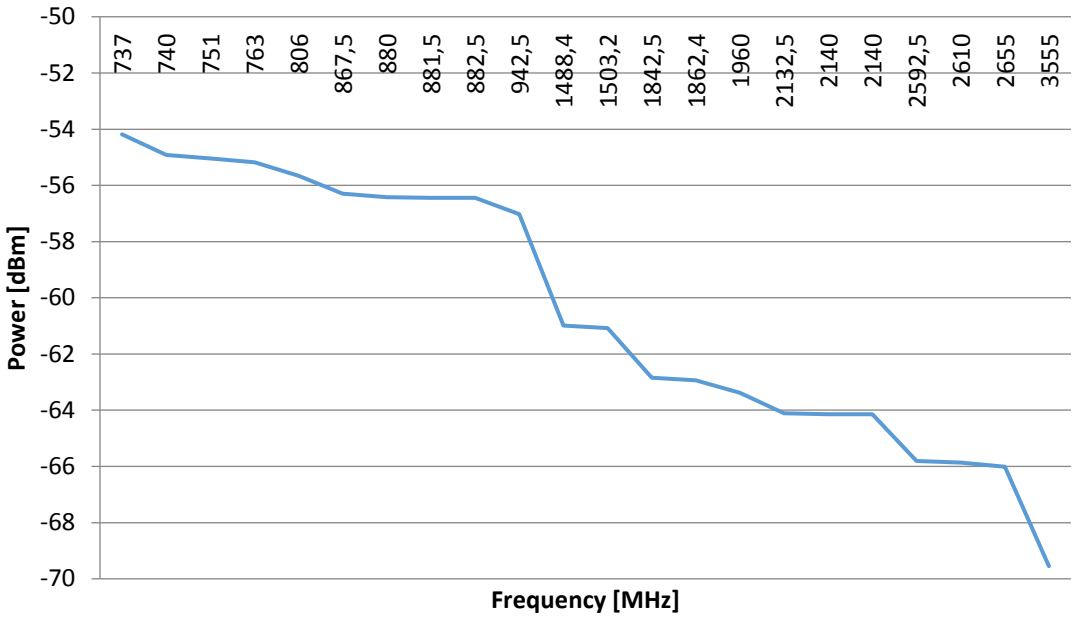

Figure 4.3 – Power received by the UE [dBm] considering free space attenuation

It is also necessary to consider the power transmitted in the uplink, *i.e.*, the power received by the eNB, according to the Equation 4.7:

$$P_{r_{eNB[dBm]}} = EIRP_{UE[dBm]} - A_{0_{up[dB]}} \tag{4.7}$$

The obtained values are shown in Figure 4.4 and Table C.3 in Annex C. When analysing Figure 4.3 and Figure 4.4, despite both curves have almost the same behaviour, the difference between the power received in the uplink and the power received in the downlink is notorious. This happens because the EIRP considered for the UE and the eNB are substantially different, being the first 23 dBm [netseminar.stanford.edu, 2012] and the latter 56.5 dBm [Sesia, *et al.*, 2009]. These values are fixed and were obtained in the respective references. It makes sense when taking into account that UEs, because of their limitations, cannot emit much power, contrarily to the eNB.

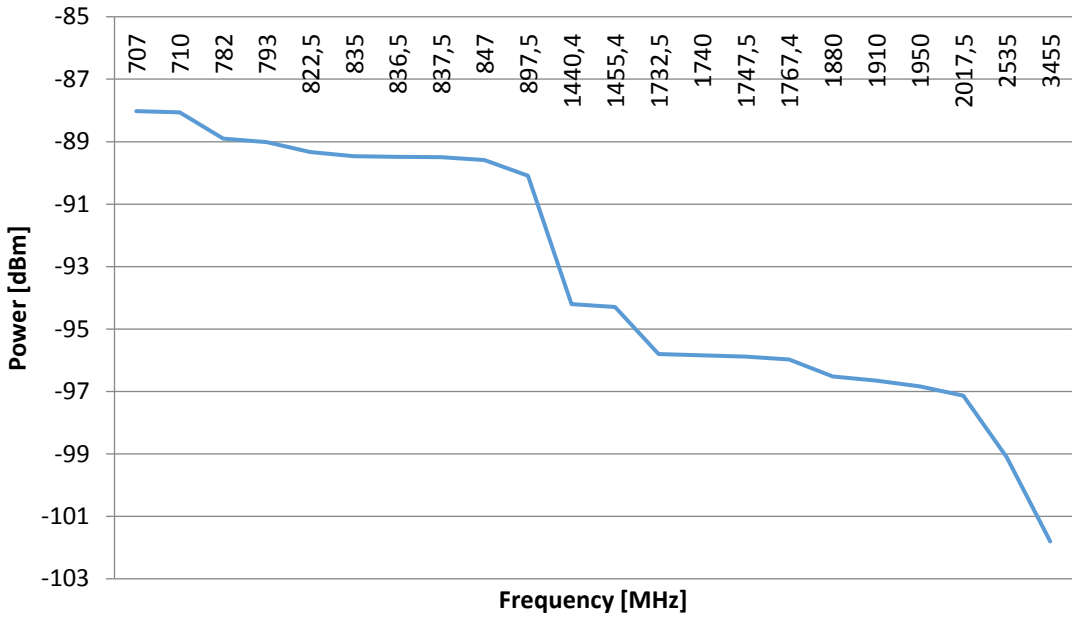

Figure 4.4 – Power received by the eNB [dBm] considering free space attenuation

As explained in more detail in Chapter 2, LTE uses OFDM in the downlink and it is possible to choose one of the three types of modulation [radio-electronics.com, 2012]:

QPSK ✈ 2 bits/symbol

16QAM ✈ 4 bits/symbol

64QAM ✈ 6 bits/symbol

For each one of these modulations, a code rate was selected – ½, ⅔ and ¾, respectively [Sesia *et al*, 2009]. The channel bandwidths considered for this work were the 1.4, 5 and 20 MHz, since the other ones were not relevant; it was enough to have the narrower, the wider and some bandwidth in the middle of those to understand the behaviour of the system.

Considering the data available in Table C.4 in Annex C, it is possible to get the REFSENS (reference sensitivity) value, which is the received power threshold, i.e., the minimum mean received signal strength applied to both antenna ports, at which SINR has a value such that it is sufficient for the specified modulation scheme to fulfil the minimum throughput requirement of 95% of the maximum possible. This is measured having the transmitter operating at full power [Sesia *et al.*, 2009].

Equation 4.8 shows how to get the REFSENS value; $k \cdot T \cdot B$ represents the thermal noise introduced, according to a specific bandwidth (here represented by B), where k stands for the Boltzmann constant (1.38065 x 10-23 J/K), T for the temperature of the receiver (which, according to [Sesia *et al.*, 2009], has the typical value of 288 degrees Kelvin) and B is a specified

noise bandwidth obtained multiplying the number of resource blocks per 180 kHz (the bandwidth of one resource block). The number of resource blocks according to each channel bandwidth can be seen in Table 4.3.

Channel bandwidth [MHz]	Number of resource blocks
1.4	7
3	15
5	25
10	50
15	75
20	100

Table 4.3 - Channel bandwidths available in LTE and respective number of resource blocks

NF is the receiver Noise Figure and measures the degradation of the SINR that is caused in the RF signal chain by components. Some examples include antenna filter losses, the degradation of the signal due to imperfections of the analogue part of the receiver, the noise introduced by the Analogue to Digital Converter (ADC), and other noise sources.

There is a requirement for *NF* in LTE; its value should be 9 dB for the UE, just like in UMTS. As far as the eNodeB is concerned, its *NF* value should be 5 dB.

SINR varies in accordance to the modulation and coding scheme, as well as IM that is the Implementation Margin, which also varies according to the modulation and coding scheme (Table C.4). The -3 dB that appears in the equation is representative of the diversity gain [Sesia *et al.*, 2009].

$$REFSENS_{[dBm]} = k \cdot T \cdot B + NF + SINR + IM - 3 \tag{4.8}$$

Knowing the REFSENS value and the EIRP calculated previously, there are conditions to calculate the maximum attenuation the signal may suffer without prejudice to the information in downlink, through:

$$at_{down_{\max}} = \frac{eirp_{eNB}}{refsens_{UE}} \tag{4.9}$$

Analogously, for the uplink:

$$at_{up_{\max}} = \frac{eirp_{UE}}{refsens_{eNB}} \tag{4.10}$$

It is easily noticed that the values obtained for the maximum attenuation the signal may suffer are higher than the ones obtained for the free space path loss. This means there is margin for the signal to suffer more attenuation than what it suffers in free space, without prejudice to the information.

With these values it is now possible to find out what is the maximum attainable distance both for uplink and downlink, according to the different frequencies, bandwidths (this time it was only considered the narrower and wider bandwidths) and modulations. These distances are listed in Table C.5 in Annex C and were obtained through the generic equation:

$$d_{\max[km]} = 10^{\frac{At_{MAX[dB]} - 20\cdot\log_{10} f_{[MHz]} - 32.4}{20}} \tag{4.11}$$

The last two lines of the table show the maximum and minimum possible distance between aircraft and UE for each of the modulations, bandwidths and frequencies. In a first glance it can be noticed that for the uplink, when using the highest frequency, the reference value for distance between aircraft and user (12 km) is not satisfied, which means the communication would not succeed under these conditions.

However, when analysing the table, it can be seen that in the downlink this is not a problem, because the minimum value obtained was approximately 22 km, when using the highest frequency, the highest modulation index and the highest bandwidth available.

This difference in the performance of the system for uplink and downlink is understandable because of the values of the emitted power; as stated earlier in this chapter, the eNB can emit much more power than the UE, due to the many implications this would have.

Once again it can be observed that when using the lowest frequency, the best results are achieved in terms of distance. As the modulation index and the bandwidth increases, the maximum distance decreases. The combination of these three factors determines the maximum distance so that the communication can be established between eNB and UE in a feasible way.

The aircraft can communicate farthest (approximately 2169 km) when operating with the lowest frequency (737 MHz), the QPSK modulation and the narrowest band (5MHz). Obviously this will have consequences as far as the bit rate is concerned. Therefore, the maximum capacity of the different channels was analysed.

For each modulation and channel bandwidth, it is possible to obtain the respective downlink bitrate when using either NCP (Normal Cyclic Prefix) or ECP (Extended Cyclic Prefix):

$$R_{DL[bps]} = \frac{NRB \cdot NSC \cdot NBS \cdot NS \cdot Cod}{D_{Slot}} \quad (4.12)$$

Where *NRB* is the number of resource blocks, *NSC* is the number of subcarriers, *NBS* is the number of bits per symbol, *NS* is the number of subcarriers, *Cod* is the code rate and D_{Slot} is the duration of the slot.

In order to make this analysis it has to be taken into account the number of resource blocks that vary according to the channel bandwidth considered, as previously listed in Table 4.3 and other elements listed in Table 4.4.

Subcarriers/ /resource block	**Bits/symbol**			**Number of symbols**		**Code rate**	**D_{slot}**
	QPSK	**16QAM**	**64QAM**	**NCP**	**ECP**		
12	2	4	6	7	6	1/3	0.0005
						2/3	
						3/4	

Table 4.4 – Necessary elements to calculate the downlink bitrate

With these elements it is possible to finally build Table 4.5, applying Equation 4.12. These results regard the use of NCP and ECP.

Downlink Bitrate [bps]						
QPSK ⅓						
B = 1.4 MHz	**B = 3 MHz**	**B = 5 MHZ**	**B = 10 MHz**	**B = 15 MHz**	**B = 20 MHz**	
784000	1680000	2800000	5600000	8400000	11200000	***NCP***
672000	1440000	2400000	4800000	7200000	9600000	***ECP***
16QAM 2/3						
B = 1.4 MHz	**B = 3 MHz**	**B = 5 MHZ**	**B = 10 MHz**	**B = 15 MHz**	**B = 20 MHz**	
3136000	6720000	11200000	22400000	33600000	44800000	***NCP***
2688000	5760000	9600000	19200000	28800000	38400000	***ECP***
64QAM 3/4						
B = 1.4 MHz	**B = 3 MHz**	**B = 5 MHZ**	**B = 10 MHz**	**B = 15 MHz**	**B = 20 MHz**	
5292000	11340000	18900000	37800000	56700000	75600000	***NCP***
4536000	9720000	16200000	32400000	48600000	64800000	***ECP***

Table 4.5 – Downlink bitrate for each modulation, channel bandwidths and considering NCP and ECP

The next step is the analysis of the channel capacity for each one of the possible bandwidths and respective modulations. As previously stated, this system has its better performance when operating at 737 MHz, therefore the calculus regard only this frequency. Results are listed in Table C.6 in Annex C.

This table shows the channel capacity for the 1.4 MHz, 5 MHz and 20 MHz bandwidths. Some values were attributed to *d* in order to compare the power received at this distance and the REFSENS value. If the first is lower than the latter, it means the system will not operate, according to the definition of REFSENS previously described; if so, the channel capacity is zero, which means it is impossible to establish communication.

The channel capacity is given by:

$$C_{[bps]} = B \cdot \log_2\left(\frac{p_r}{n}\right) \tag{4.13}$$

where B is the channel bandwidth, p_r is the received power and n is the noise. In order to obtain the value of the received power it is necessary to apply the equation:

$$p_r = \frac{eirp}{l_0} \tag{4.14}$$

where *eirp* is the effective isotropic radiated power and l_0 is the free space attenuation, which can be obtained by:

$$l_0 = \left(\frac{4\pi df}{c} \right)^2 \tag{4.15}$$

where *d* is replaced by the predefined values for distance listed in Table C.6, *f* is the 737 MHz frequency and *c* is the speed of light.

With the values from Table C.6 three graphics were built for better comprehension and easier analysis of the results. They are represented in Figure 4.5, Figure 4.6 and Figure 4.7.

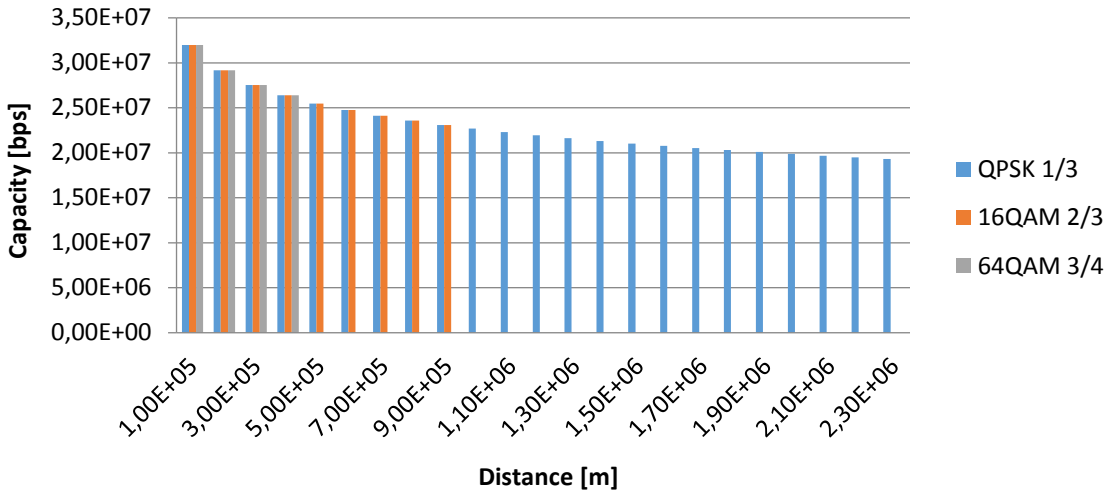

Figure 4.5 - Capacity of the 1.4 MHz channel according to distance between aircraft and UE

Considering f = 737 MHz and for a 1.4 MHz bandwidth channel, this graphic illustrates the capacity of the channel, whilst the distance between UE and eNB increases, regarding the three modulations studied in this dissertation. It can be observed that the 64QAM modulation will not work for distances longer than 400 km and 16 QAM can be used for distances not exceeding 900 km. The low power needed for it to work (when comparing to other modulations) allows QPSK to perform at distances such as 2300 km. However, this implies that the capacity of the channel is highly affected. If at 100 km away it is possible to have approximately 32 Mbps, at 2300 km away the best one can get is a little above 19 Mbps.

These values are substantially different from the maximum download speed of 100 Mbps expected from LTE systems. However, this is not a bad result at all considering the distances achieved.

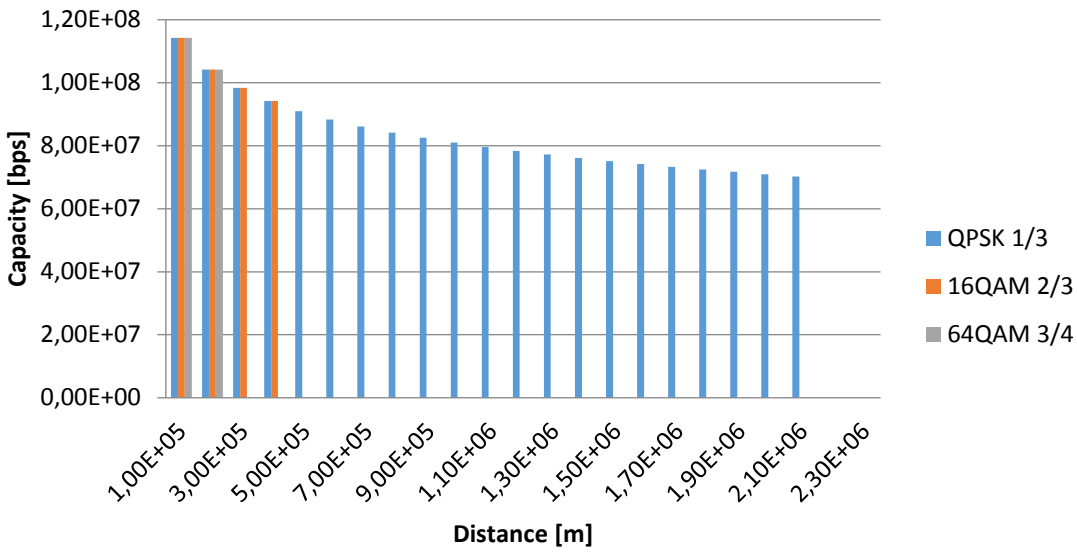

Figure 4.6 - Capacity of the 5 MHz channel according to distance between aircraft and UE

Considering the same elements as in the previous graphic with exception for the bandwidth, which is 5 MHz in this case, several interesting observations can be made; the maximum distance that can separate aircraft from UE is 2110 km, approximately 200 km less than in the previous case. Another difference lies in the fact that all three modulations only operate if UE is no more than 200 km away from the aircraft, 16QAM operates until it reaches 400 km of distance, and QPSK operates until reaching 2100 km.

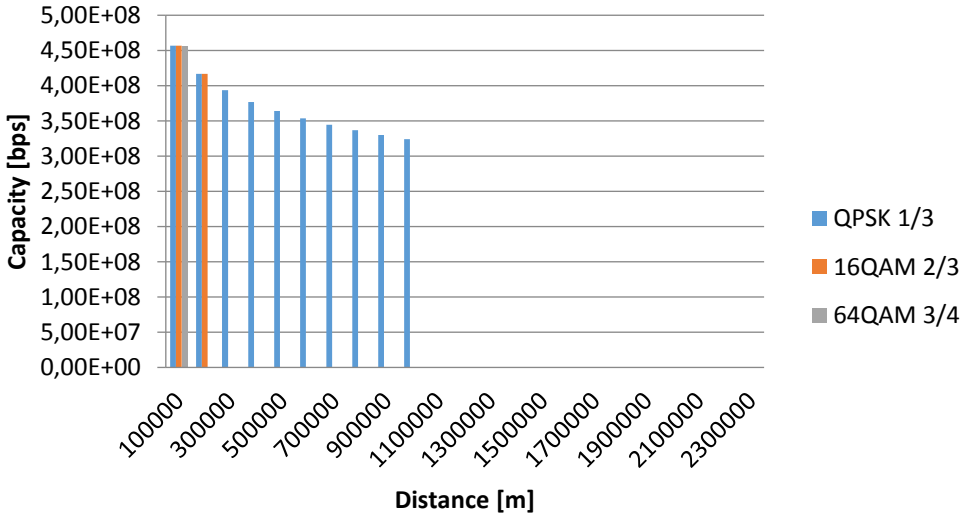

Figure 4.7 - Capacity of the 5 MHz channel according to distance between aircraft and UE

This graphic shows that the maximum attainable distance is 1000 km when considering the 20 MHz channel. Also, it can be seen that the 64QAM modulation can only be used when the aircraft is 100 km away from the user equipment, and 16QAM can be used when the distance reaches the value of 200 km. QPSK can be used until 1000 km. In the best case scenario, *i.e.*, when the aircraft is 100 km away from the user equipment, the channel has approximately 457 Mbps of capacity. On the other hand, it has 323 Mbps of capacity when considering QPSK and a distance of 1000 km.

As main conclusion after observing these graphics and tables, it can be stated that for now - that it is only being taken into account the propagation of the signal in free space - the system works. However, its performance depends on the modulation, frequency and channel bandwidth chosen.

Next some graphics are represented depicting the relation between the received power and the distance that separates UE and eNB (Figure 4.8 to Figure 4.11). There are other influencing factors taken into account, like modulation scheme and channel bandwidth chosen. Data used to build these graphics is gathered in Table C.7 in Annex C.

The received power according to distance when using the QPSK modulation and for a REFSENS value of approximately -100 dBm, which corresponds to the 5 MHz channel, is represented in Figure 4.8. The vertical purple line in the graphic represents the boundary imposed by the REFSENS. This means that all received signals which power has a value below -100 dBm should be ignored since the system will not operate. Hence, it is clearly noticeable that, once again, the 737 MHz frequency provides the best performance when compared to higher frequencies such as 2140 MHz and 3555 MHz. With these frequencies it is possible to communicate up to 750 km and 450 km respectively.

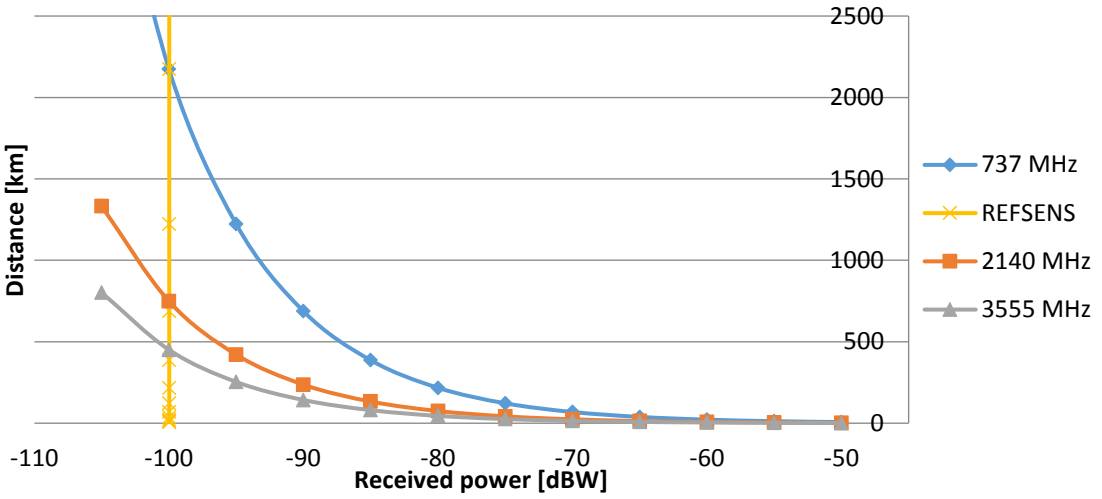

Figure 4.8 – Received power according to distance using QPSK and having REFSENS of approximately -100 dBW

When considering QPSK modulation and a 20 MHz channel, the value of REFSENS increases to approximately -93.95 dBm. The same frequencies were analysed and the same criteria used as in the previous case. The results are listed in Table C.9 and depicted in Figure 4.9.

In this case the 737 MHz frequency allows communications to be established from approximately 1200 km away, 2140 MHz from 380 km and 3555 MHz from 120 km. These values are substantially lower than the ones obtained for the previous case because, despite the use of the same modulation, this time it is being used a four times superior bandwidth.

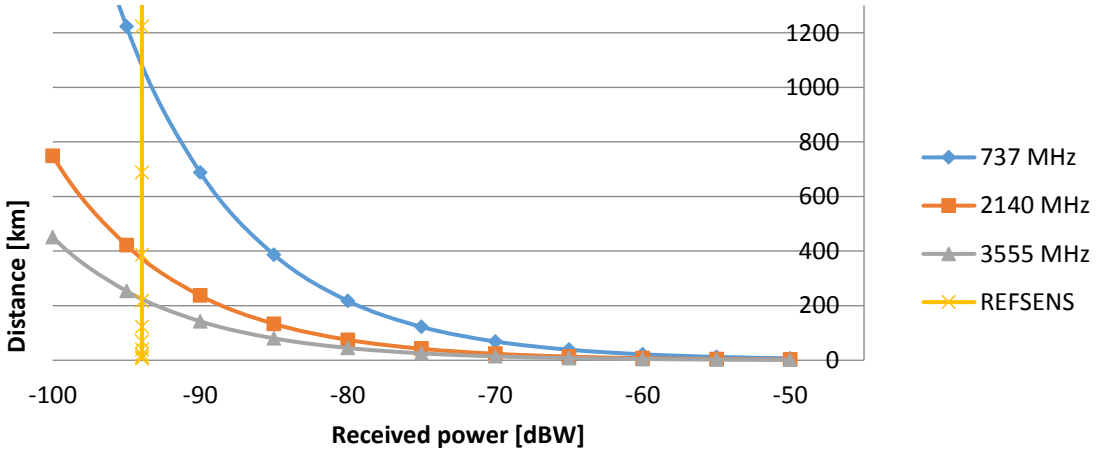

Figure 4.9 - Received power according to distance using QPSK and having REFSENS of approximately -94 dBW

Once again it is the performance of the 737 MHz frequency that stands out among the others studied. When the received power equals the REFSENS value (-80 dBm), it means that the eNB is, at most, approximately 1200 km away from the UE if the system is operating in the 737 MHz frequency, 400 km if operating in the 2140 MHz and 250 km if operating in the 3555 MHz frequency. These results are similar to the ones obtained in the previous case although the modulation is now 64QAM and not QPSK. This happens because in this case the channel bandwidth is 5 MHz. It is expected that increasing the bandwidth will make these values decrease.

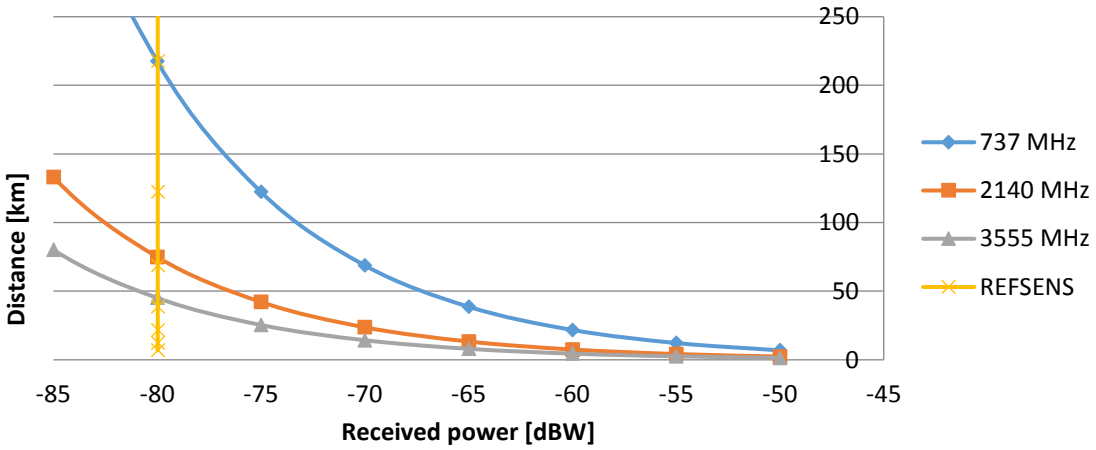

Figure 4.10 - Received power according to distance using 64QAM and having REFSENS of approximately -80 dBW

Considering 64QAM and a 20 MHz channel, the REFSENS value comes to the highest value of -74 dBm. As expected, the impact of a high modulation index – 64QAM – combined with a large bandwidth – 20 MHz – brings consequences as far as distances are concerned. Thus, approximately 120 km is the farthest the UE may be so he can receive signal from the aircraft, when is being used the 737 MHz frequency, 38 km if using the 2140 MHz frequency and 12 km if using the 3555 MHz frequency.

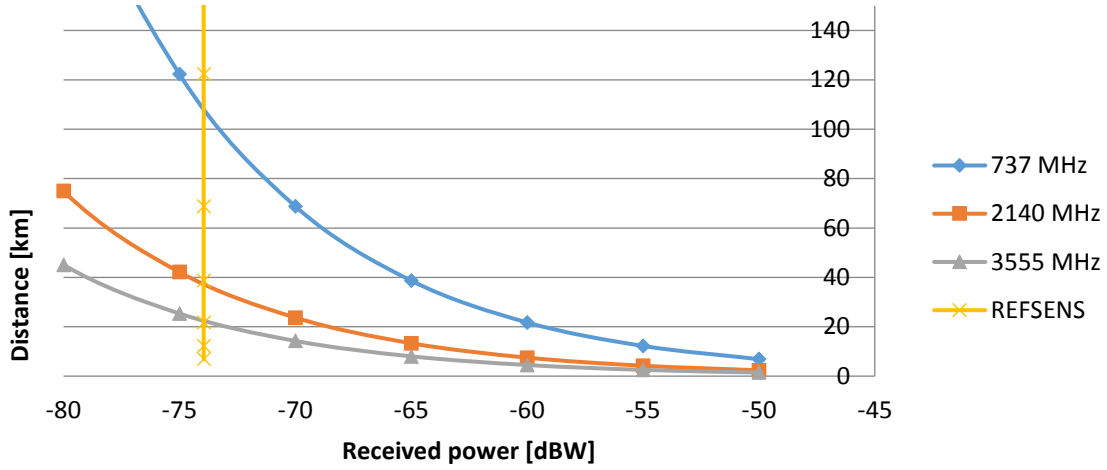

Figure 4.11 - Received power according to distance using 64QAM and having REFSENS of approximately -74 dBW

In general, the graphics above represent an expected situation that also occurs with terrestrial base stations; they show that the UE receives more power in shorter distances, *i.e.*, when it is closer to the aircraft. This situation also occurs when the UE is near a terrestrial BS, as the UE moves away from the BS the power received also decreases. The abrupt end of line noticeable in all graphics is due to the value of attributed power to the system. They all start at -50 dBm because this is the maximum power received by the UE.

4.2.2 Propagation with obstacles

In spite of the existence of some line of sight parts in the transmission path, there are also some parts severely obstructed by obstacles, such as mountains, buildings and foliage, for instance. These constraints have to be taken into account since they will cause damage in the transmitted signal, which can be severe or even fatal in some cases.

To ascertain a value for this attenuation, it has to be considered the fact that there are different surroundings and environments around the globe. There are large cities like New York, Tokyo and London with many buildings and huge skyscrapers that constitute serious threats to any wireless communication, but there are also deserts, small villages and cities that are harmless and offer little attenuation besides the free space path loss.

It is possible to identify three different outdoor environments, usually associated to distinct propagation models [Vieira, 2005]. The terrain undulation, vegetation and buildings density, the existence of open areas, the existence of aquatic surfaces, among other aspects, are

crucial for the classification of each environment. The environments can be classified as shown in Figure 4.12.

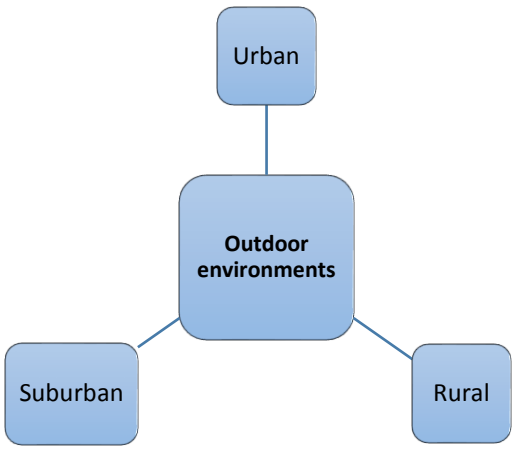

Figure 4.12 – Outdoor environments classification

In a rural environment (Figure 4.13) there are wider areas and a smaller density of buildings, which is beneficial for the propagation of the signal and its prediction. However, it is possible the coexistence of an enormous density of vegetation which, in turn, can lead to a great attenuation, damaging the signal.

Figure 4.13– Rural environment

Suburban environments (Figure 4.14) are characterized by a mix of rural and urban environments. In this case, the terrain is occupied by a greater density of constructions, yet the existence of open areas prevails.

Figure 4.14– Suburban environment

In the case of an urban environment (Figure 4.15), the enormous density of buildings will result in the existence of many reflections, which conducts to fading. The attenuation of the signal by reflection, diffraction, scattering or refraction depends on the construction materials. Owing to the characteristics of this environment, having a propagation model based on real measurements becomes extremely complicated, and there may be significant deviations between predictions and the real signal [Varela, 2009].

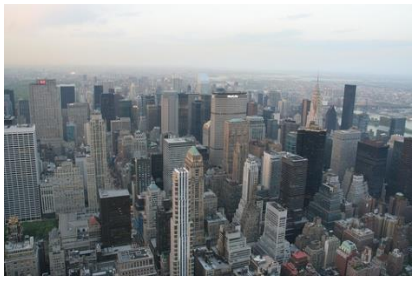

Figure 4.15 – Urban environment

Because of the inexistence of a generic propagation model that contemplates all the possible environments, frequencies and other specific parameters in this system, it was necessary to consider the creation of a new propagation model to deduce the average attenuation. This model is represented in Equation 4.16:

$$\overline{PL}(d,\theta,f) = A_0 + \left[10\cdot\gamma\cdot\log\left(\frac{d}{d_0}\right) + 6\cdot\log\left(\frac{f}{2000}\right) + s\right]\cdot\cos(\theta)\cdot\left[u(\theta) - u(\theta-\theta_{env})\right] \quad (4.16)$$

where $A_0 = 20\cdot\log\left(\frac{4\pi d}{\lambda}\right)$, the expression aforementioned when the values for free space path loss were calculated. γ is the path loss exponent and varies according to the environment; its possible values are listed in Table 4.6. d refers to the distance that separates UE and eNB, which is 12000 m and d_0 stands for the reference distance, which is 100 m. f is for frequency and it was decided to study only the 737 MHz frequency, since it was the one that provided the best performance to the system. s is a log normally distributed factor that is used to account for the shadow fading owing to trees and other clutter, and has a value of 9.4 dB. θ is the angle the aircraft does with respect to the UE and θenv is the angle according to the environment, *i.e.*, for each environment there is a threshold value for θ which is θenv. When the aircraft is at some given distance from the UE, it is different if they are in an urban or rural environment, because the height of buildings in urban areas, for instance, may obstruct line of sight, and therefore it is necessary to consider this case. The values for θ_{env} according to the environment are listed in Table 4.7 [Montenegro-Villacieros *et al.*, 2010].

	γ
Urban (A)	4
Suburban (B)	3
Rural (C)	2

Table 4.6 – γ values according to the environment

Angles according to scenario[°]		
θenv$_A$	**θenv$_B$**	**θenv$_C$**
70	60	40

Table 4.7 – Maximum possible angles according to scenario

This propagation model has three important components, which are: A_0, representing the free space attenuation, $\left[10\cdot\gamma\cdot\log\left(\frac{d}{d_0}\right)+6\cdot\log\left(\frac{f}{2000}\right)+s\right]$ representing the attenuation due to obstacles, and $\cos(\theta)\cdot\left[u(\theta)-u\left(\theta-\theta_{env}\right)\right]$ that represents the angle the aircraft does with respect to the UE and its impact in the signal.

The results achieved for the path loss using this model are illustrated in Figure 4.16. As expected, the urban environment is the one that offers more attenuation to the signal, followed by the suburban, and the rural environment appears as the least damaging in terms of attenuation. It can be observed that as the angle increases towards the threshold angle, the value for attenuation decreases, since it means the aircraft is approaching the UE to a point where there is line of sight between them, therefore the value for attenuation is the same as if they were in free space.

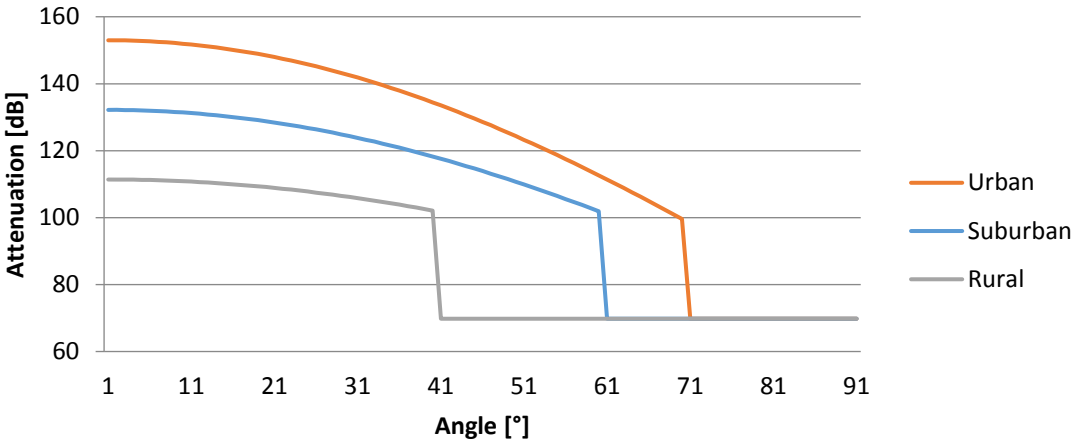

Figure 4.16 – Path loss when using 737 MHz frequency according to model in Equation 4.16

It is possible to manipulate Equation 4.16 to solve it and obtain *d*, having the value for path loss, angle and frequency, as demonstrated in Annex C.2. The result is Equation 4.17.

$$d = \left[10^{\frac{PL - 6\cdot\log\left(\frac{f}{2000}\right)\cdot\cos(\theta)\cdot\left[u(\theta)-u(\theta-\theta_{env})\right] - s\cdot\cos(\theta)\cdot\left[u(\theta)-u(\theta-\theta_{env})\right]}{10}} \cdot \frac{\lambda^2 \cdot {d_0}^{\gamma\cdot\cos(\theta)\cdot\left[u(\theta)-u(\theta-\theta_{env})\right]}}{16\cdot\pi^2} \right]^{\frac{1}{2+\gamma\cdot\cos(\theta)\cdot\left[u(\theta)-u(\theta-\theta_{env})\right]}}$$

(4.17)

With this equation it is possible to elaborate a study of the behaviour of the system. The following graphics, from Figure 4.18 to Figure 4.26, give a better idea of the functioning and performance of the system, since they illustrate the maximum distance attainable in the three different environments when operating with the lowest frequency, *i.e.*, 737 MHz and considering the three modulations studied along the project. The graphics are referring to the 1.4 MHz, 5 MHz and 20 MHz channel bandwidth. The slope visible in all graphics happens when the angle the aircraft does with respect to the UE matches θ_{env}, which in practice means that the threshold angle for that environment was reached and from that angle on, the aircraft is in line of sight with the UE, therefore the path loss is the same as verified when analysing the transmission in free space.

Having the maximum distance and knowing the values for θ_{env} according to the environment, it is possible to draw a triangle with these elements as depicted in Figure 4.17:

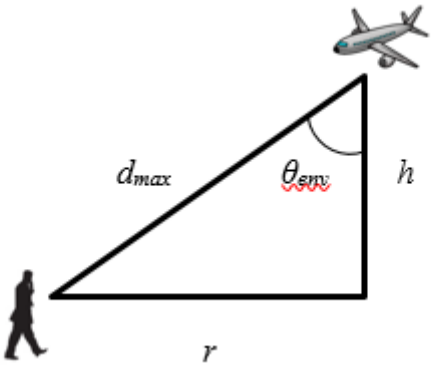

Figure 4.17 – Geometry of the communication between aircraft and UE

Despite the Earth has a round shape, because these measures are so small comparing to the Earth, it is assumed that the cathetus represented by *r* is linear. This *r* represents the approximate value of the radius of the cell, and will vary according to the environment and the particularities of the communication (modulation, channel bandwidth, frequency).

Applying basic concepts of trigonometry, the value of *r* can be found by:

$$r = d_{\max} \cdot \sin\left(\theta_{env}\right) \tag{4.18}$$

Urban environment

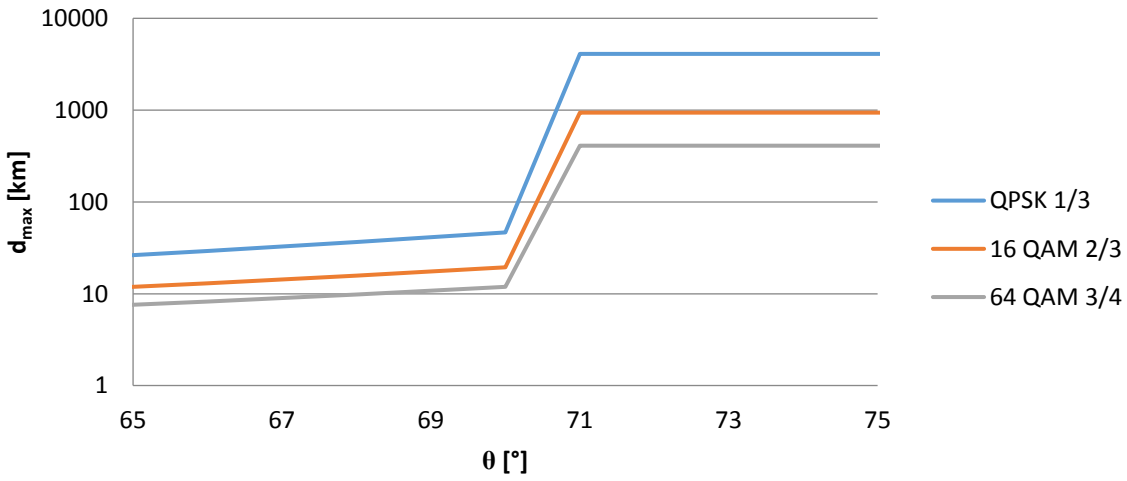

Figure 4.18 – Maximum distance in urban environment having

B = 1.4 MHz and f = 737 MHz

	QPSK	16QAM	64QAM
d_{max}[km]	29.04	12.6	2.64

Table 4.8 – Maximum distance when θ reaches the value of θ_{env} according to Figure 4.18

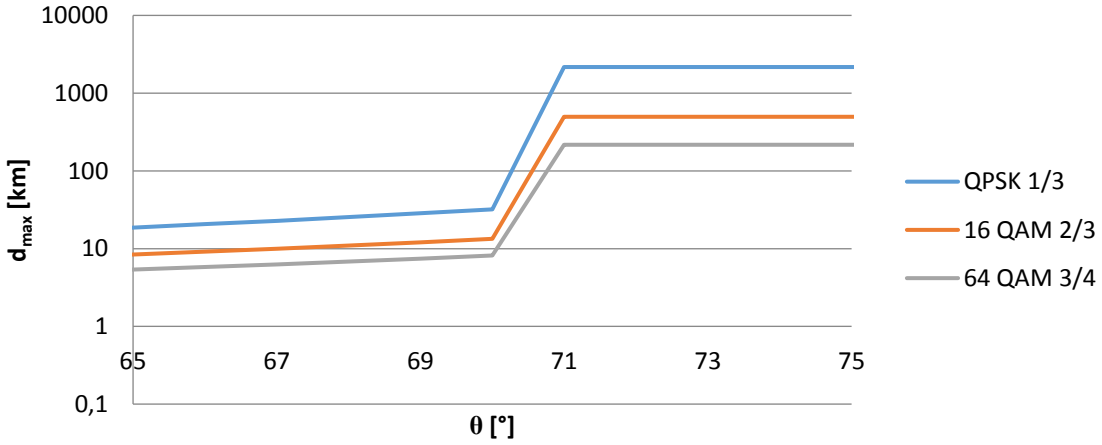

Figure 4.19 – Maximum distance in urban environment having B = 5 MHz and f = 737 MHz

	QPSK	16QAM	64QAM
d_{max}[km]	20.25	5.50	5.50

Table 4.9 – Maximum distance when θ reaches the value of θ_{env} according to Figure 4.19

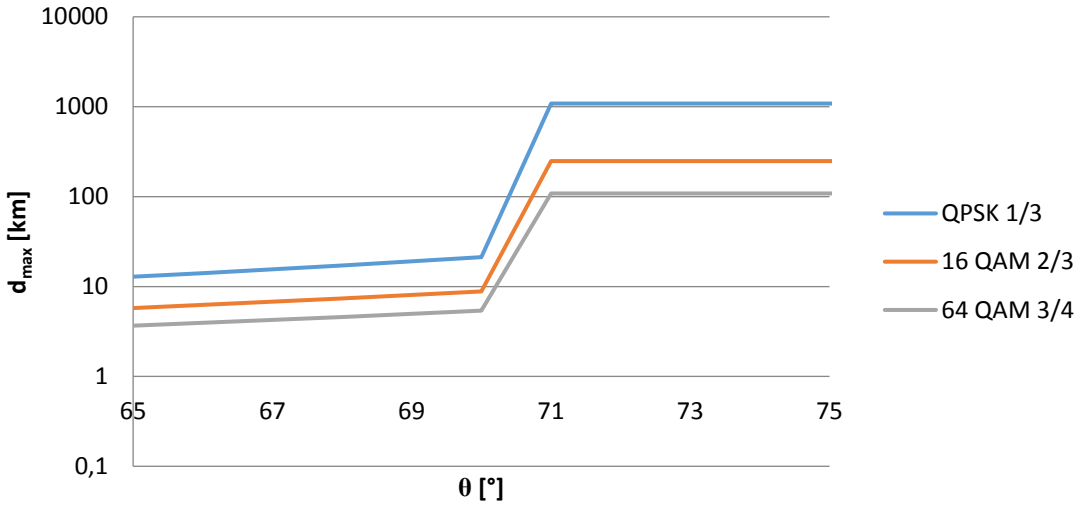

Figure 4.20 – Maximum distance in urban environment having
B = 20 MHz and f = 737 MHz

	QPSK	16QAM	64QAM
d_{max}[km]	5.94	3.71	3.71

Table 4.10 – Maximum distance when θ reaches the value of θ_{env} according to Figure 4.20

In urban scenario, the value of d_{max} the moment θ reaches the value of θ_{env}, varies from 29.04 km when using QPSK and for a channel bandwidth of 1.4 MHz, and 3.71 km when using 64QAM and for a channel bandwidth of 20 MHz. This means that, applying Equation 4.18, the value of r, the approximate cell radius, will vary from 18.67 km and 2.38 km, respectively.

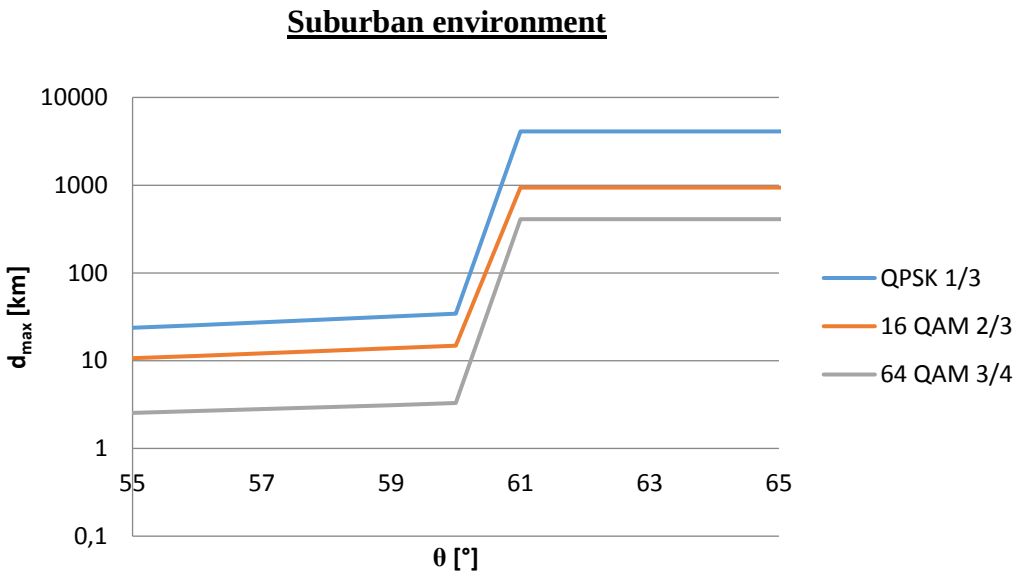

Figure 4.21 – Maximum distance in suburban environment having B = 1.4 MHz and f = 737 MHz

	QPSK	16QAM	64QAM
d_{max}[km]	34.46	14.84	3.29

Table 4.11 – Maximum distance when θ reaches the value of θ_{env} according to Figure 4.21

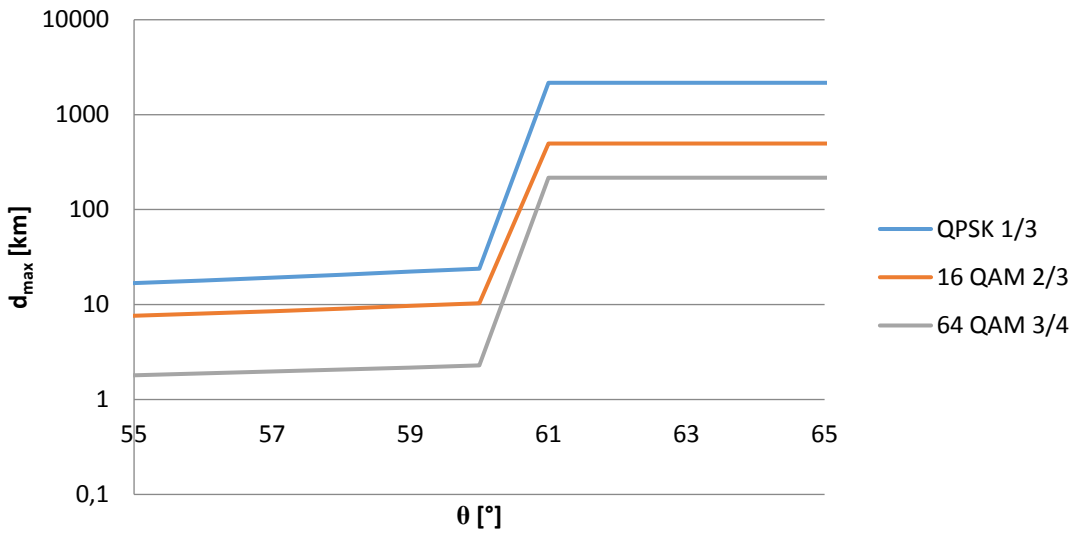

Figure 4.22 – Maximum distance in suburban environment having B = 5 MHz and f = 737 MHz

	QPSK	16QAM	64QAM
d_{max}[km]	23.95	10.32	2.28

Table 4.12 – Maximum distance when θ reaches the value of θ_{env} according to Figure 4.22

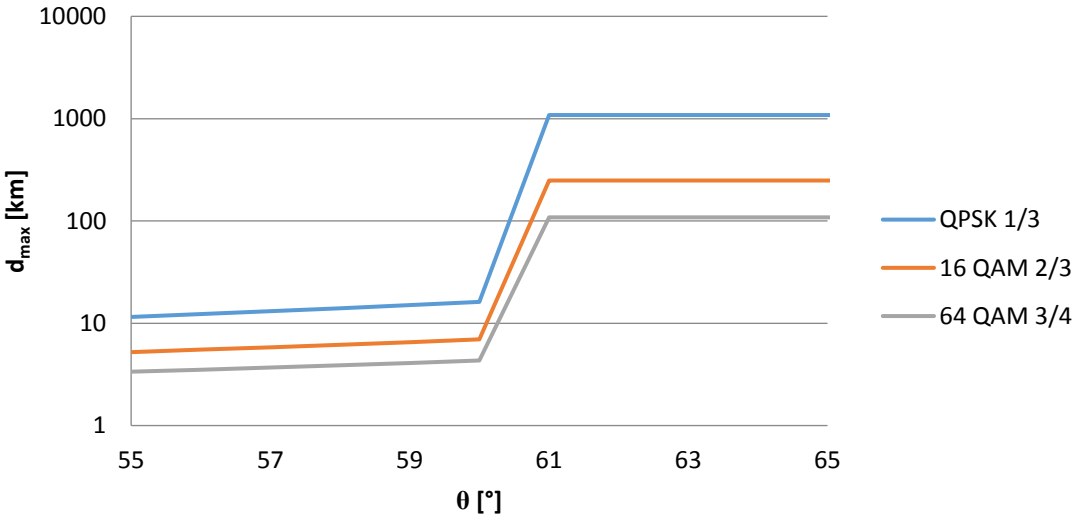

Figure 4.23 – Maximum distance in suburban environment having B = 20 MHz and f = 737 MHz

	QPSK	16QAM	64QAM
d_{max}[km]	16.12	6.94	4.32

Table 4.13 – Maximum distance when θ reaches the value of θ_{env} according to Figure 4.23

In suburban scenario, the value of d_{max} the moment θ reaches the value of θ_{env}, varies from 34.46 km when using QPSK and for a channel bandwidth of 1.4 MHz, and 4.32 km when using 64QAM and for a channel bandwidth of 20 MHz. This means that, applying Equation 4.18, the value of r, the approximate cell radius, will vary from 29.84 km and 3.74 km, respectively.

Rural environment

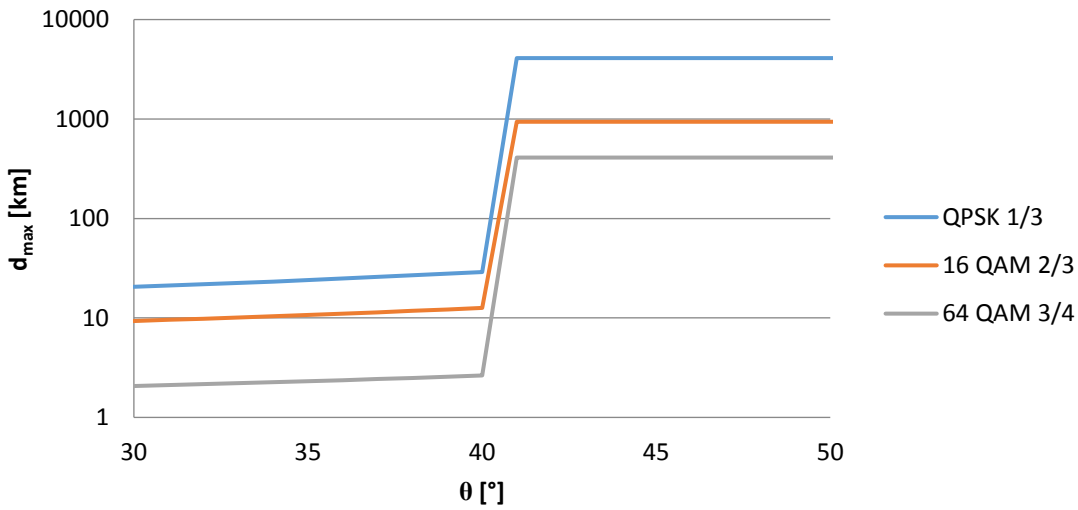

Figure 4.24 – Maximum distance in rural environment having B = 1.4 MHz and f = 737 MHz

	QPSK	16QAM	64QAM
d_{max}[km]	46.62	19.43	11.88

Table 4.14 – Maximum distance when θ reaches the value of θ_{env} according to Figure 4.24

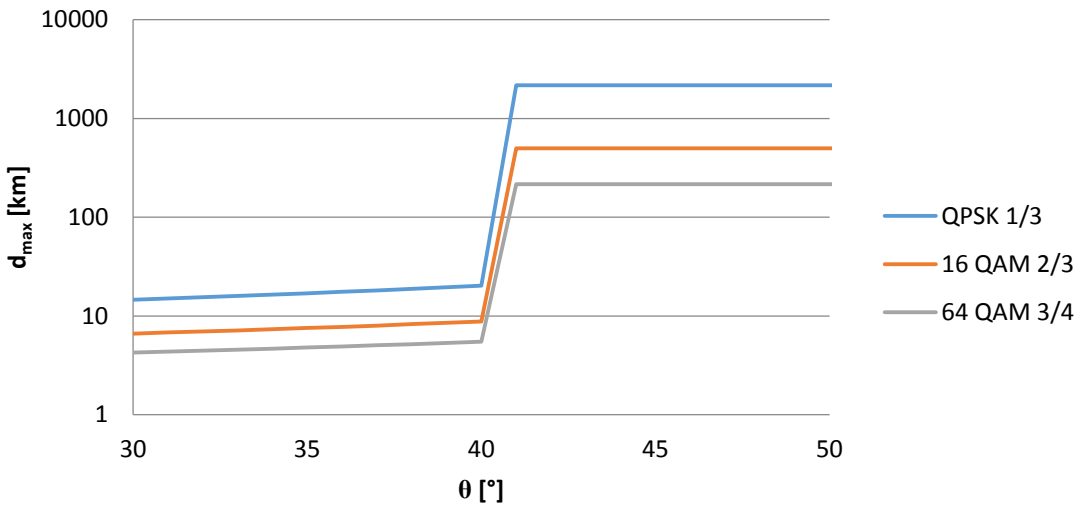

Figure 4.25 – Maximum distance in rural environment having
B = 5 MHz and f = 737 MHz

	QPSK	16QAM	64QAM
d_{max}[km]	31.95	13.32	8.14

Table 4.15 – Maximum distance when θ reaches the value of θ_{env} according to Figure 4.25

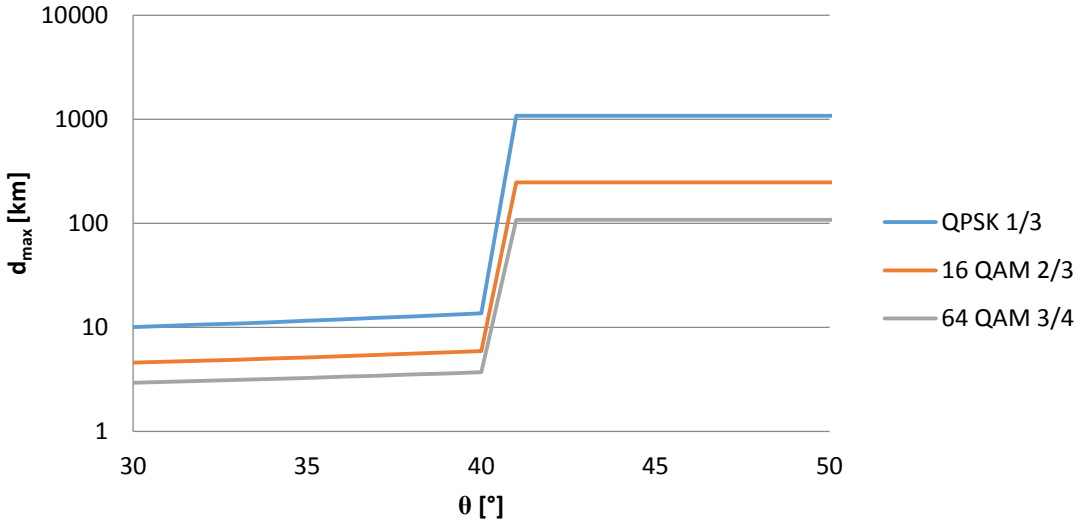

Figure 4.26 – Maximum distance in rural environment having
B = 20 MHz and f = 737 MHz

	QPSK	16QAM	64QAM
d_{max}[km]	21.17	8.82	5.93

Table 4.16 – Maximum distance when θ reaches the value of θ_{env} according to Figure 4.26

In rural scenario, the value of d_{max} the moment θ reaches the value of θ_{env}, varies from 46.62 km when using QPSK and for a channel bandwidth of 1.4 MHz, and 5.93 km when using 64QAM and for a channel bandwidth of 20 MHz. This means that, applying Equation 4.18, the value of *r*, the approximate cell radius, will vary from 43.80 km and 5.57 km, respectively.

After this analysis, lies the idea that the cells in rural environment are quite bigger than the ones in urban scenario. If choosing one modulation and then proceed to analyse its behaviour in the three different scenarios, it is visible that when using the same modulation, the cells have bigger radius when in rural scenario and smaller in urban scenario.

In the following graphics (Figure 4.27 – Figure 4.29) it is represented the power received by the UE in the three different environments, according to the angle between the aircraft and the UE. The frequency in use is 737 MHz. The horizontal curves represent the REFSENS values for the three different channel bandwidths analysed – 1.4 MHz, 5 MHz and 20 MHz. When the curves relating to the environments are below the horizontal lines of REFSENS, it means the value of the received power is lower than the threshold value for the power received; therefore, there is not enough power to establish communication. In all graphics, when the curves relating to the environments reach their respective θ_{env}, the received power automatically increases to values referent to the received power when communicating in free space.

In the particular case of Figure 4.27, illustrating the received power when using QPSK modulation, it is visible that when using this modulation, communication can be established in all environments and using any channel bandwidth with exception for the urban environment and B = 20 MHz, where it is only possible to communicate when the angle between the aircraft and the UE is approximately 13° or higher.

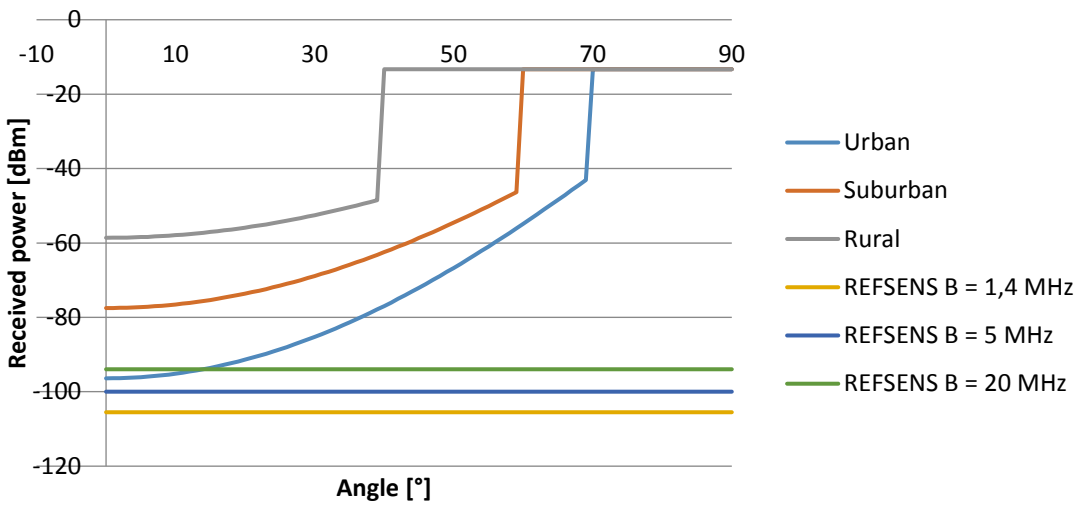

Figure 4.27 – Received power in different environments according to angle for QPSK [dBm]

Regarding Figure 4.28, representing received power when using 16QAM, once again it is only the urban environment the one having limitations. This time, all channel bandwidths are affected. To communicate using B = 1.4 MHz it is necessary that θ has a value of approximately 17° or higher; using B = 5 MHz, θ has to be approximately 28° or higher, and to communicate using a channel with 20 MHz bandwidth, θ has to be approximately 36° or higher.

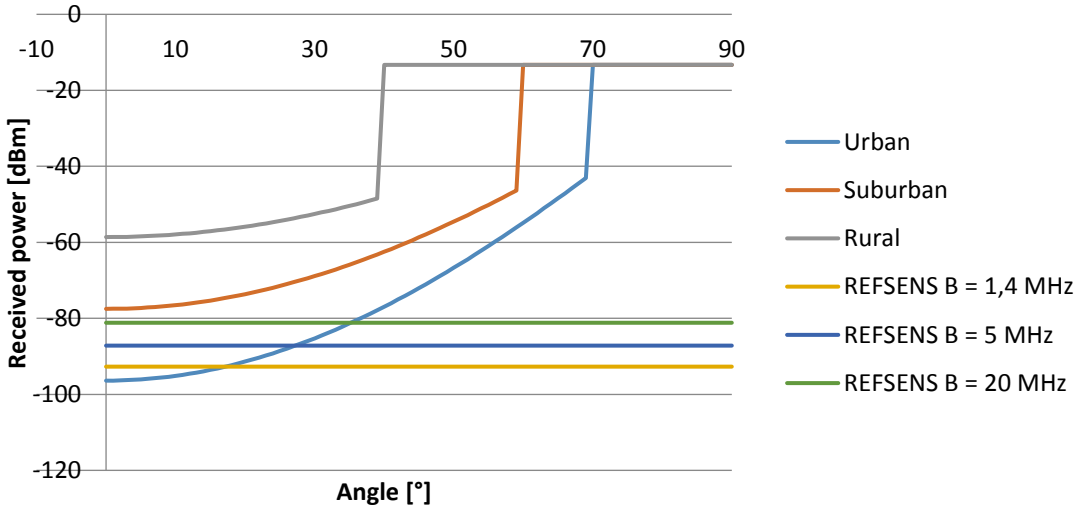

Figure 4.28 – Received power in different environments according to angle for 16QAM [dBm]

Because of its accuracy comparing to the previous modulations, the 64QAM modulation is the most limiting, and in this case besides the urban environment, the suburban environment also presents its limitations, as can be seen in Figure 4.29.

As far as the urban environment is concerned, it presents limitations when communicating using any of the three channel bandwidths; when in urban environment and when B = 1.4 MHz, it is necessary that θ has a value of 30° or higher; when B = 5 MHz, θ has to have the value of 37° or higher, and when B = 20 MHz θ has to have the minimum value of 44°.

In suburban environment the only limitation that exists is when using the 20 MHz channel bandwidth. In this case it is necessary that θ has a value of 20° or higher.

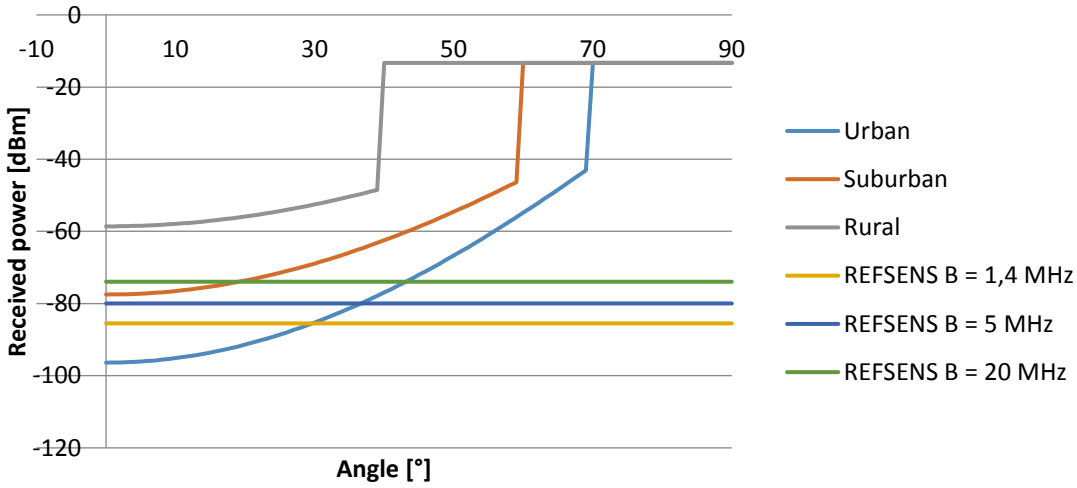

Figure 4.29 – Received power in different environments according to angle for 64QAM [dBm]

Considering the geometry presented in Figure 4.30, representing two hypothetical buildings separated by a street or avenue, it is possible to calculate the estimated value of the angle θ, having the values of the height of the building (H) and half of the width of the street (W). This can be done with the use of random variables.

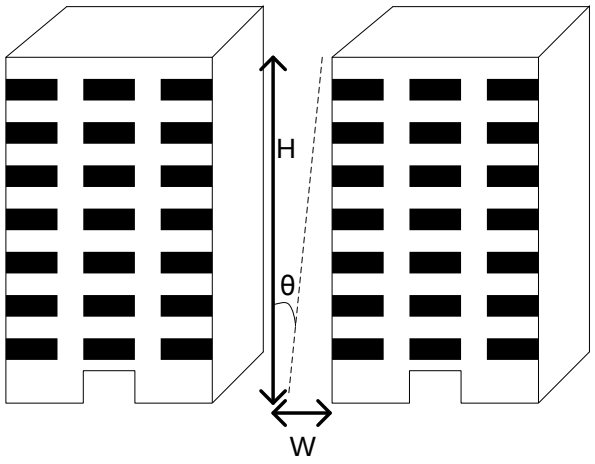

Figure 4.30 – Some important elements to calculate the estimated value of θ

Considering:

$$\tan(\theta) = \frac{W}{H} \tag{4.19}$$

$$z = \tan(\theta) \tag{4.20}$$

$$g(z) = \arctan(\theta) \Rightarrow g'(z) = \frac{d\arctan(z)}{dz} = \frac{1}{1+z^2} \tag{4.21}$$

$$p_Z(z) = \int_{-\infty}^{+\infty} |h| \cdot p_W(h \cdot z) \cdot p_H h \tag{4.22}$$

$$p_{\theta_{env}}(\theta_{env}) = \frac{p_Z(z)}{\left|\frac{d\theta_{env}}{dz}\right|} = \frac{p_Z(z)}{|g'(z)|}\Bigg|_{z=g^{-1}} \tag{4.23}$$

$$p_{\theta env}(\theta_{env}) = \frac{1}{\left|\frac{1}{1+\left[\tan(\theta_{env})\right]^2}\right|} \cdot p_Z(\tan\theta_{env}) \tag{4.24}$$

$$p_{\theta_{env}}(\theta_{env}) = \left|1+\left[\tan(\theta_{env})\right]^2\right| \cdot \int_0^{+\infty} |h| \cdot p_W(h \cdot z) \cdot p_H(h)\, dh \tag{4.25}$$

The mean value of the angle is given by equation (4.26):

$$E\left[\theta_{env}\right] = \int_{0}^{\frac{\pi}{2}} \theta_{env} \cdot p_{\theta_{env}}\left(\theta_{env}\right) d\theta_{env} \Leftrightarrow$$

$$\Leftrightarrow E\left[\theta_{env}\right] = \int_{0}^{\frac{\pi}{2}} \int_{0}^{+\infty} \theta_{env} \cdot \left|1+\tan\left(\theta_{env}\right)^{2}\right| \cdot |h| \cdot p_{W}\left(h \cdot z\right) \cdot p_{H}\left(h\right) dh d\theta_{env} \Leftrightarrow$$

$$\Leftrightarrow E\left[\theta_{env}\right] = \int_{0}^{\frac{\pi}{2}} \int_{0}^{+\infty} \theta_{env} \cdot \left|1+\tan\left(\theta_{env}\right)^{2}\right| \cdot |h| \cdot p_{W}\left(h \cdot \tan\left(\theta_{env}\right)\right) \cdot p_{H}\left(h\right) dh d\theta_{env} \quad (4.26)$$

This is particularly interesting because it can be applied to any location; having the average height and street width measures of any given place, the typical value for the angle in that scenario can be obtained.

Chapter 5

Conclusions and Future Work

This is the final chapter where the main conclusions are presented, as well as some suggestions for future work in order to take this project to the next level.

5.1 Conclusions

The objective of this dissertation was the characterization of a global 4G mobile communications network, supported by commercial aircrafts.

From the work developed in this dissertation, the main conclusion is that it is possible to establish a communication between a flying aircraft and a UE that is located in the ground. One of the most concerning aspects in a project involving aircrafts – especially if it is a communications project – is the frequencies used, so that no interference occurs. In Chapter 3 it was clarified that the frequencies used in LTE do not clash with the ones used in aeronautical communications in a way that this project becomes unfeasible.

In Chapter 4 the propagation of the signal was studied in terms of attenuation with and without obstacles. Inclusively, a propagation model was deduced especially for these propagation conditions taking into account the different environments where the signal can be transmitted. The power received by the UE was calculated after all the loss suffered due to the attenuation and it was concluded that depending on the environment, the power received – in theory – is different. If the UE is in urban environment the power received will be less than if it is in suburban environment, and if it is in suburban environment the power received will be less than if it is in rural environment. The modulation has a dominant role in the performance of the system, since its combination with the channel bandwidth is crucial when it comes to the bitrate achieved.

As far as the network is concerned, LTE SON system consists basically on a software package to be incorporated into a network. Because networks are growing in complexity, it is important to simplify their management and SON appeared exactly to meet this requirement. Also, another important fact is that it enables the efficiency of the network to increase, while keeping the costs low. Because of its simplicity and the efficiency it entails, it seems like the perfect concept to be implemented in a network composed by aircrafts. A very complex network, intended to be managed as simply as possible, given its unique characteristics.

5.2 Future work

This is a very challenging project that can be divided into many tasks. Some of them were successfully accomplished, but due to the extension and complexity of this theme, there is a lot of work that needs to be done to conclude that this is a feasible project.

It is necessary to check the cell sizes in each one of the environments and thereafter, by the speed of the aircrafts, predict the time of handover.

Also, because of the speed of the aircrafts, it is of paramount importance to solve the Doppler problem. Because aircrafts move so fast, Doppler shift introduced in the signal will certainly be devastating to the communication, therefore it is necessary to study and adjust the suitable compensation technique to this system.

Regarding the network, a more detailed study has to be done in order to find the convenient architecture and means of functioning, so that the best performance can be achieved. It would be interesting to have this network operating together with terrestrial and satellite networks in order to improve the overall capacity of the available communications networks.

Once all the theoretical studies are concluded it would be important to develop a prototype to perform some studies and measures on the field. However, entities like ICAO (International Civil Aviation Organization), responsible for the safety of civil aviation, may offer some resistance because of the aforementioned concern with projects involving communications and aircrafts.

Annex A

A.1 – Auxiliary Tables for Chapter 2 and Chapter 4

LTE Band Number	Uplink [MHz]	Downlink [MHz]
1	1920-1980	2110-2170
2	1850-1910	1930-1990
3	1710-1785	1805-1880
4	1710-1755	2110-2155
5	824-849	869-894
6	830-840	875-885
7	2500-2570	2620-2690
8	880-915	925-960
9	1749,9-1784,9	1844,9-1879,9
10	1710-1770	2110-2170
11	1427,9-1452,9	1475,9-1500,9
12	698-716	728-746
13	777-787	746-756
14	788-798	758-768
15	1900-1920	2600-2620
16	2010-2025	2585-2600
17	704-716	734-746
18	815-830	860-875
19	830-845	875-890
20	832-862	791-821
21	1447,9-1462,9	1495,5-1510,9
22	3410-3500	3510-3600
23	2000-2020	2180-2200
24	1625,5-1660,5	1525-1559
25	1850-1915	1930-1995

Table A.1 – FDD bands and frequencies

Source [radio-electronics.com, 2012]

LTE Band Number	Allocation [MHz]
33	1900-1920
34	2010-2025
35	1850-1910
36	1930-1990
37	1910-1930
38	2570-2620
39	1880-1920
40	2300-2400
41	2496-2690
42	3400-3600
43	3600-3800

Table A.2 – TDD bands and frequencies

Source [radio-electronics.com, 2012]

Annex B

B.1 – Auxiliary Table for Chapter 3

Rank	Airport	Location	Code (IATA/ICAO)	Total passengers
1.	Hartsfield–Jackson Atlanta International Airport	Atlanta, Georgia, USA	ATL/KATL	103,902,992
2.	Beijing Capital International Airport	Chaoyang-Shunyi, Beijing, China	PEK/ZBAA	95,786,442
3.	Dubai International Airport	Garhoud, Dubai, United Arab Emirates	DXB/OMDB	88,242,099
4.	Tokyo Haneda Airport	Ōta, Tokyo, Japan	HND/RJTT	85,408,975
5.	Los Angeles International Airport	Los Angeles, California, USA	LAX/KLAX	84,557,968
6.	O'Hare International Airport	Chicago, Illinois, USA	ORD/KORD	79,828,183
7.	London Heathrow Airport	Hillingdon, London, UK	LHR/EGLL	78,014,598
8.	Hong Kong International Airport	Chek Lap Kok, Hong Kong, China	HKG/VHHH	72,665,078
9.	Shanghai Pudong International Airport	Pudong, Shanghai, China	PVG/ZSPD	70,001,237
10.	Paris-Charles de Gaulle Airport	Roissy-en-France, Île-de-France, France	CDG/LFPG	69,471,442
11.	Amsterdam Airport Schiphol	Haarlemmermeer, North Holland, Netherlands	AMS/EHAM	68,515,425
12.	Dallas/Fort Worth International Airport	Dallas-Fort Worth, Texas, USA	DFW/KDFW	67,092,194
13.	Guangzhou Baiyun International Airport	Baiyun-Huadu, Guangzhou, Guangdong, China	CAN/ZGGG	65,887,473
14.	Frankfurt Airport	Frankfurt, Hesse, Germany	FRA/EDDF	64,500,386
15.	Istanbul Atatürk Airport	Yeşilköy, Istanbul, Turkey	IST/LTBA	63,859,785
16.	Indira Gandhi International Airport	Delhi, India	DEL/VIDP	63,451,503
17.	Soekarno-Hatta International Airport	Tangerang, Banten, Indonesia	CGK/WIII	63,015,620
18.	Singapore Changi Airport	Changi, Singapore	SIN/WSSS	62,219,573
19.	Seoul Incheon International Airport	Incheon, Republic of Korea	ICN/RKSI	62,157,834
20.	Denver International Airport	Denver, Colorado, USA	DEN/KDEN	61,379,396

Table B.1 - Busiest airports in the world by passenger traffic

Source: [Wikipedia.org, 2018b]

Annex C

C.1 – Auxiliary Tables for Chapter 4

A_{0up} [dB]	$A_{0\ down}$ [dB]
119,834	120,642
119,517	119,879
118,882	119,342
118,807	120,611
112,483	112,938
112,467	112,923
122,113	122,515
113,094	113,519
118,980	119,435
118,845	120,642
117,203	117,488
111,022	111,383
111,898	111,546
112,019	111,684
119,654	122,366
120,130	122,308
111,059	111,418
112,336	112,799
112,493	112,948
112,591	112,160
117,293	117,573
124,803	125,050

Table C.1 – Free space attenuation values for uplink (A_{0up}) and downlink (A_{0down})

Power received by the UE	
[dBm]	**[linear]**
-64,142	3,853E-10
-63,379	4,593E-10
-62,842	5,198E-10
-64,111	3,880E-10
-56,438	2,279E-09
-56,423	2,279E-09
-66,015	2,503E-10
-57,019	1,986E-09
-62,935	5,087E-10
-64,142	3,853E-10
-60,988	7,965E-10
-54,883	3,249E-09
-55,046	3,129E-09
-55,184	3,031E-09
-65,866	2,590E-10
-65,808	2,625E-10
-54,918	3,222E-09
-56,299	2,345E-09
-56,448	2,266E-09
-55,660	2,716E-09
-61,074	7,809E-10
-69,550	1,396E-10

Table C.2 – Power received by the UE considering free space attenuation only

Power received by the aircraft (eNB)	
[dBm]	**[linear]**
-96,834	2,073E-13
-96,517	2,230E-13
-95,882	2,581E-13
-95,807	2,626E-13
-89,483	1,126E-12
-89,467	1,130E-12
-99,113	1,227E-13
-90,094	9,785E-13
-95,980	2,523E-13
-95,845	2,603E-13
-94,203	3,799E-13
-88,022	1,577E-12
-88,898	1,289E-12
-89,019	1,253E-12
-96,654	2,160E-13
-97,130	1,936E-13
-88,059	1,564E-12
-89,336	1,165E-12
-89,493	1,123E-12
-89,591	1,099E-12
-94,293	3,721E-13
-101,803	6,603E-14

Table C.3 – Power received by the eNB considering free space attenuation only

Reference sensitivity													
System	**Modulation**	**Channel BW [MHz]**	**kT B [dBm]**	**NF [dB]**	**SINR [dB]**	**IM [dB]**	**REFSENS [dBm]**	**refsens [linear]**	**eirp [linear]**	**at up max [linear]**	**At UP MAX [dB]**	**at down max [linear]**	**At DOWN MAX [dBW]**
LTE UE	QPSK ⅓	1,4	-113,0015328	9	-1	2,5	-105,5015328	2,81739E-14	0,199526231	–	–	1,58545E+16	162,001533
		5	-107,4731131	9	-1	2,5	-99,97311307	1,00621E-13				4,43927E+15	156,473113
		20	-101,4525132	9	-1	2,5	-93,95251316	4,02484E-13				1,10982E+15	150,452513
	16QAM 2/3	1,4	-113,0015328	9	11,3	3	-92,70153276	5,36842E-13				8,32057E+14	149,201533
		5	-107,4731131	9	11,3	3	-87,17311307	1,91729E-12				2,32976E+14	143,673113
		20	-101,4525132	9	11,3	3	-81,15251316	7,66918E-12				5,8244E+13	137,652513
	64QAM 3/4	1,4	-113,0015328	9	17,5	4	-85,50153276	2,81739E-12				1,58545E+14	142,001533
		5	-107,4731131	9	17,5	4	-79,97311307	1,00621E-11				4,43927E+13	136,473113
		20	-101,4525132	9	17,5	4	-73,95251316	4,02484E-11				1,10982E+13	130,452513
LTE BS	QPSK ⅓	5	-107,5	5	1,5	2,5	-101,5	7,07946E-14	446,6835922	2,81838E+12	124,5	–	–

Table C.4 – Reference sensitivity (REFSENS) values

	Maximum distance [km]							
	UE - BS	BS - UE						
f_{up} [MHz]	QPSK ⅓	QPSK ⅓	QPSK ⅓	16QAM 2/3	16QAM 2/3	64QAM 3/4	64QAM 3/4	f_{down} [MHz]
	B = 5 MHz	B = 5 MHz	B = 20 MHz	B = 5 MHz	B = 20 MHz	B = 5 MHz	B = 20 MHz	
1950	20,65215561	746,8646084	373,4323042	171,0967972	85,54839862	74,68646084	37,34323042	2140
1880	21,42111885	815,4542153	407,7271077	186,8097684	93,40488421	81,54542153	40,77271077	1960
1747,5	23,04532385	867,4574014	433,7287007	198,7230101	99,36150505	86,74574014	43,37287007	1842,5
1732,5	23,24485047	749,4913304	374,7456652	171,6985445	85,84927224	74,94913304	37,47456652	2132,5
836,5	48,14310034	1813,14834	906,5741702	415,3682883	207,6841441	181,314834	90,65741702	881,5
835	48,22958495	1816,238934	908,1194671	416,0763024	208,0381512	181,6238934	90,81194671	880
2535	15,88627354	601,9925658	300,9962829	137,9085296	68,9542648	60,19925658	30,09962829	2655
897,5	44,87097875	1695,798687	847,8993433	388,4850357	194,2425178	169,5798687	84,78993433	942,5
1767,4	22,78584555	858,1884998	429,0942499	196,5996274	98,29981371	85,81884998	42,90942499	1862,4
1740	23,14465715	746,8646084	373,4323042	171,0967972	85,54839862	74,68646084	37,34323042	2140
1440,4	27,95869441	1073,831135	536,9155677	246,0005013	123,0002506	107,3831135	53,69155677	1488,4
707	**56,96139099**	**2168,643503**	**1084,321752**	**496,8075253**	**248,4037626**	**216,8643503**	**108,4321752**	737
782	51,49834199	2128,216061	1064,108031	487,5461333	243,7730667	212,8216061	106,4108031	751
793	50,7839892	2094,744773	1047,372387	479,8783042	239,9391521	209,4744773	104,7372387	763
710	56,72070906	2159,851705	1079,925853	494,7934407	247,3967203	215,9851705	107,9925853	740
822,5	48,96255736	1842,409524	921,204762	422,0716382	211,0358191	184,2409524	92,1204762	867,5
837,5	48,08561604	1811,093781	905,5468907	414,897616	207,448808	181,1093781	90,55468907	882,5
847	47,54628504	1982,9904	991,4951998	454,2768562	227,1384281	198,29904	99,14951998	806
1455,4	27,67053967	1063,258556	531,6292782	243,5784634	121,7892317	106,3258556	53,16292782	1503,2
3455	**11,65606467**	**449,5893845**	**224,7946923**	**102,9949778**	**51,4974889**	**44,95893845**	**22,47946923**	3555
max:	56,96139099	2168,643503	1084,321752	496,8075253	248,4037626	216,8643503	108,4321752	
min:	11,65606467	449,5893845	224,7946923	102,9949778	51,4974889	44,95893845	22,47946923	

Table C.5 – Maximum attainable distances for uplink and downlink

			B [Hz] = 1400000			B [Hz] = 5000000			B [Hz] = 20000000		
			Modulation			Modulation			Modulation		
f [Hz]	7,370E+08		**QPSK 1/3**	**16QAM 2/3**	**64QAM 3/4**	**QPSK 1/3**	**16QAM 2/3**	**64QAM 3/4**	**QPSK 1/3**	**16QAM 2/3**	**64QAM 3/4**
d [m]	**l_0**	**p_r**	**Channel Capacity [bps]**			**Channel Capacity [bps]**			**Channel Capacity [bps]**		
100000	9,544E+12	4,680E-11	31978441,2	31978441,2	31978441,2	114208718,6	114208718,6	114208718,6	456834874,3	456834874,3	456834874,3
200000	3,817E+13	1,170E-11	29178442,01	29178442,01	29178442,01	104208721,4	104208721,4	104208721,4	416834885,8	416834885,8	0
300000	8,589E+13	5,200E-12	27540548,35	27540548,35	27540548,35	98359101,24	98359101,24	0	393436405	0	0
400000	1,527E+14	2,925E-12	26378445,23	26378445,23	26378445,23	94208732,96	94208732,96	0	376834931,9	0	0
500000	2,386E+14	1,872E-12	25477048,98	25477048,98	0	90989460,65	0	0	363957842,6	0	0
600000	3,436E+14	1,300E-12	24740555,6	24740555,6	0	88359127,15	0	0	353436508,6	0	0
700000	4,676E+14	9,552E-13	24117860,31	24117860,31	0	86135215,41	0	0	344540861,6	0	0
800000	6,108E+14	7,313E-13	23578458,13	23578458,13	0	84208779,02	0	0	336835116,1	0	0
900000	7,730E+14	5,778E-13	23102672,69	23102672,69	0	82509545,32	0	0	330038181,3	0	0
1000000	9,544E+14	4,680E-13	22677069,13	0	0	80989532,62	0	0	323958130,5	0	0
1100000	1,155E+15	3,868E-13	22292064,91	0	0	79614517,54	0	0	0	0	0
1200000	1,374E+15	3,250E-13	21940584,62	0	0	78359230,78	0	0	0	0	0
1300000	1,613E+15	2,769E-13	21617255,13	0	0	77204482,6	0	0	0	0	0
1400000	1,871E+15	2,388E-13	21317899,81	0	0	76135356,47	0	0	0	0	0
1500000	2,147E+15	2,080E-13	21039207,72	0	0	75140027,56	0	0	0	0	0
1600000	2,443E+15	1,828E-13	20778509,71	0	0	74208963,27	0	0	0	0	0
1700000	2,758E+15	1,620E-13	20533622,63	0	0	73334366,52	0	0	0	0	0
1800000	3,092E+15	1,445E-13	20302737,98	0	0	72509778,5	0	0	0	0	0
1900000	3,445E+15	1,297E-13	20084340,89	0	0	71729788,89	0	0	0	0	0
2000000	3,817E+15	1,170E-13	19877149,74	0	0	70989820,49	0	0	0	0	0
2100000	4,209E+15	1,061E-13	19680070,64	0	0	70285966,56	0	0	0	0	0
2200000	4,619E+15	9,670E-14	19492162,44	0	0	0	0	0	0	0	0
2300000	5,049E+15	8,848E-14	19312609,59	0	0	0	0	0	0	0	0

Table C.6 – Channel capacity according to the channel bandwidth when using f = 737 MHz

		n_0	N_0 [dBW]	N_0 [dBm]	N	N	p_r	s/n	S/N	C [Mbps]					
										a)	b)	c)	d)	e)	f)
f [MHz]	728-746	4,47761E-19	-175,068	-145,068	-142,058	6,2264E-18	3,24865E-09	521753995,5	87,175	579,176	434,382	289,588	144,794	86,876	40,542
	2110-2170	1,80421E-17	-170,402	-140,402	-137,391	1,82333E-17	3,8531E-10	21132188,85	73,249	486,659	364,994	243,329	121,665	72,999	34,066
	3510-3555	2,98544E-17	-168,225	-138,225	-135,215	3,00969E-17	1,39623E-10	4639129,568	66,664	442,908	332,181	221,454	110,727	66,436	31,004

Nf	3,0102999
a)	20
b)	15
B[MHz] c)	10
d)	5
e)	3
f)	1,4

Table C.7 – Elements to draw the graphics related to the received power according to distance

f = 737 [MHz]			f = 2140 [MHz]			f = 3555 [MHz]		
Pr [dBW]	**At [dB]**	**d [Km]**	**Pr [dBW]**	**At [dB]**	**d [Km]**	**Pr [dBW]**	**At [dB]**	**d [Km]**
-50	106,5	6,879114088	-50	106,5	2,369115459	-50	106,5	1,4261342
-55	111,5	12,23298694	-55	111,5	4,212949241	-55	111,5	2,536065085
-60	116,5	21,7536688	-60	116,5	7,491800891	-60	116,5	4,509832323
-65	121,5	38,68410132	-65	121,5	13,32251527	-65	121,5	8,019741962
-70	126,5	68,79114088	-70	126,5	23,69115459	-70	126,5	14,261342
-75	131,5	122,3298694	-75	131,5	42,12949241	-75	131,5	25,36065085
-80	136,5	217,536688	-80	136,5	74,91800891	-80	136,5	45,09832323
-85	141,5	386,8410132	-85	141,5	133,2251527	-85	141,5	80,19741962
-90	146,5	687,9114088	-90	146,5	236,9115459	-90	146,5	142,61342
-95	151,5	1223,298694	-95	151,5	421,2949241	-95	151,5	253,6065085
-100	156,5	2175,36688	-100	156,5	749,1800891	-100	156,5	450,9832323
-105	161,5	3868,410132	-105	161,5	1332,251527	-105	161,5	801,9741962

Table C.8 – Attenuation and distance for a given received power and three different frequencies when using the 5 MHz channel and QPSK modulation

f = 737 [MHz]			f = 2140 [MHz]			f = 3555 [MHz]		
Pr [dBW]	**At [dB]**	**d [Km]**	**Pr [dBW]**	**At [dB]**	**d [Km]**	**Pr [dBW]**	**At [dB]**	**d [Km]**
-50	106,5	6,879114088	-50	106,5	2,369115459	-50	106,5	1,4261342
-55	111,5	12,23298694	-55	111,5	4,212949241	-55	111,5	2,536065085
-60	116,5	21,7536688	-60	116,5	7,491800891	-60	116,5	4,509832323
-65	121,5	38,68410132	-65	121,5	13,32251527	-65	121,5	8,019741962
-70	126,5	68,79114088	-70	126,5	23,69115459	-70	126,5	14,261342
-75	131,5	122,3298694	-75	131,5	42,12949241	-75	131,5	25,36065085
-80	136,5	217,536688	-80	136,5	74,91800891	-80	136,5	45,09832323
-85	141,5	386,8410132	-85	141,5	133,2251527	-85	141,5	80,19741962
-90	146,5	687,9114088	-90	146,5	236,9115459	-90	146,5	142,61342
-95	151,5	1223,298694	-95	151,5	421,2949241	-95	151,5	253,6065085
-100	156,5	2175,36688	-100	156,5	749,1800891	-100	156,5	450,9832323
-105	161,5	3868,410132	-105	161,5	1332,251527	-105	161,5	801,9741962

Table C.9 – Attenuation and distance for a given received power and three different frequencies when using the 20 MHz channel and QPSK modulation

f = 737 [MHz]			f = 2140 [MHz]			f = 3555 [MHz]		
Pr [dBW]	**At [dB]**	**d [Km]**	**Pr [dBW]**	**At [dB]**	**d [Km]**	**Pr [dBW]**	**At [dB]**	**d [Km]**
-50	106,5	6,879114088	-50	106,5	2,369115459	-50	106,5	1,4261342
-55	111,5	12,23298694	-55	111,5	4,212949241	-55	111,5	2,536065085
-60	116,5	21,7536688	-60	116,5	7,491800891	-60	116,5	4,509832323
-65	121,5	38,68410132	-65	121,5	13,32251527	-65	121,5	8,019741962
-70	126,5	68,79114088	-70	126,5	23,69115459	-70	126,5	14,261342
-75	131,5	122,3298694	-75	131,5	42,12949241	-75	131,5	25,36065085
-80	136,5	217,536688	-80	136,5	74,91800891	-80	136,5	45,09832323
-85	141,5	386,8410132	-85	141,5	133,2251527	-85	141,5	80,19741962
-90	146,5	687,9114088	-90	146,5	236,9115459	-90	146,5	142,61342
-95	151,5	1223,298694	-95	151,5	421,2949241	-95	151,5	253,6065085
-100	156,5	2175,36688	-100	156,5	749,1800891	-100	156,5	450,9832323
-105	161,5	3868,410132	-105	161,5	1332,251527	-105	161,5	801,9741962

Table C.10 – Attenuation and distance for a given received power and three different frequencies when using the 5 MHz channel and 64QAM modulation

f = 737 [MHz]			f = 2140 [MHz]			f = 3555 [MHz]		
Pr [dBW]	**At [dB]**	**d [Km]**	**Pr [dBW]**	**At [dB]**	**d [Km]**	**Pr [dBW]**	**At [dB]**	**d [Km]**
-50	106,5	6,879114088	-50	106,5	2,369115459	-50	106,5	1,4261342
-55	111,5	12,23298694	-55	111,5	4,212949241	-55	111,5	2,536065085
-60	116,5	21,7536688	-60	116,5	7,491800891	-60	116,5	4,509832323
-65	121,5	38,68410132	-65	121,5	13,32251527	-65	121,5	8,019741962
-70	126,5	68,79114088	-70	126,5	23,69115459	-70	126,5	14,261342
-75	131,5	122,3298694	-75	131,5	42,12949241	-75	131,5	25,36065085
-80	136,5	217,536688	-80	136,5	74,91800891	-80	136,5	45,09832323
-85	141,5	386,8410132	-85	141,5	133,2251527	-85	141,5	80,19741962
-90	146,5	687,9114088	-90	146,5	236,9115459	-90	146,5	142,61342
-95	151,5	1223,298694	-95	151,5	421,2949241	-95	151,5	253,6065085
-100	156,5	2175,36688	-100	156,5	749,1800891	-100	156,5	450,9832323
-105	161,5	3868,410132	-105	161,5	1332,251527	-105	161,5	801,9741962

Table C.11 – Attenuation and distance for a given received power and three different frequencies when using the 20 MHz channel and 64QAM modulation

C.2 – Propagation Model Deduction

$$\overline{PL} = A_0 + \left[10 \cdot \gamma \cdot \log\left(\frac{d}{d_0} \right) + 6 \cdot \log\left(\frac{f}{2000} \right) + s \right] \cdot \cos(\theta) \cdot \left[u(\theta) - u(\theta - \theta_{env}) \right] \Leftrightarrow$$

$$\Leftrightarrow \overline{PL} = 20 \cdot \log\left(\frac{4 \cdot \pi \cdot d}{\lambda} \right) + \left[10 \cdot \gamma \cdot \log\left(\frac{d}{d_0} \right) + 6 \cdot \log\left(\frac{f}{2000} \right) + s \right] \cdot \cos(\theta) \cdot \left[u(\theta) - u(\theta - \theta_{env}) \right] \Leftrightarrow$$

$$\Leftrightarrow \overline{PL} = 20 \cdot \log\left(\frac{4 \cdot \pi \cdot d}{\lambda} \right) + 10 \cdot \gamma \cdot \log\left(\frac{d}{d_0} \right) \cdot \cos(\theta) \cdot \left[u(\theta) - u(\theta - \theta_{env}) \right] +$$

$$+ 6 \cdot \log\left(\frac{f}{2000} \right) \cdot \cos(\theta) \cdot \left[u(\theta) - u(\theta - \theta_{env}) \right] + s \cdot \cos(\theta) \cdot \left[u(\theta) - u(\theta - \theta_{env}) \right] \Leftrightarrow$$

$$\Leftrightarrow \overline{PL} - 6 \cdot \log\left(\frac{f}{2000} \right) \cdot \cos(\theta) \cdot \left[u(\theta) - u(\theta - \theta_{env}) \right] - s \cdot \cos(\theta) \cdot \left[u(\theta) - u(\theta - \theta_{env}) \right] =$$

$$= 20 \cdot \log\left(\frac{4 \cdot \pi \cdot d}{\lambda} \right) + 10 \cdot \gamma \cdot \log\left(\frac{d}{d_0} \right) \cdot \cos(\theta) \cdot \left[u(\theta) - u(\theta - \theta_{env}) \right]$$

Considering:

$$A = \overline{PL} - 6 \cdot \log\left(\frac{f}{2000} \right) \cdot \cos(\theta) \cdot \left[u(\theta) - u(\theta - \theta_{env}) \right] - s \cdot \cos(\theta) \cdot \left[u(\theta) - u(\theta - \theta_{env}) \right]$$

Comes:

$$A = 10\left[\log\left(\frac{16\cdot\pi^2\cdot d^2}{\lambda^2}\right)+\gamma\cdot\log\left(\frac{d}{d_0}\right)\cdot\cos(\theta)\cdot\left[u(\theta)-u(\theta-\theta_{env})\right]\right]\Leftrightarrow$$

$$\Leftrightarrow \frac{A}{10} = \log\left(\frac{16\cdot\pi^2\cdot d^2}{\lambda^2}\right)+\gamma\cdot\log\left(\frac{d}{d_0}\right)\cdot\cos(\theta)\cdot\left[u(\theta)-u(\theta-\theta_{env})\right]\Leftrightarrow$$

$$\Leftrightarrow \frac{A}{10} = \log\left(\frac{16\cdot\pi^2\cdot d^2}{\lambda^2}\right)+\log\left(\frac{d}{d_0}\right)^{\gamma\cdot\cos(\theta)\cdot\left[u(\theta)-u(\theta-\theta_{env})\right]}\Leftrightarrow$$

$$\Leftrightarrow \frac{A}{10} = \log\left(\frac{16\cdot\pi^2\cdot d^2}{\lambda^2}\right)+\log\left(\frac{d^{\gamma\cdot\cos(\theta)\cdot\left[u(\theta)-u(\theta-\theta_{env})\right]}}{d_0^{\gamma\cdot\cos(\theta)\cdot\left[u(\theta)-u(\theta-\theta_{env})\right]}}\right)\Leftrightarrow$$

$$\Leftrightarrow \frac{A}{10} = \log\left(\frac{16\cdot\pi^2\cdot d^2\cdot d^{\gamma\cdot\cos(\theta)\cdot\left[u(\theta)-u(\theta-\theta_{env})\right]}}{\lambda^2\cdot d_0^{\gamma\cdot\cos(\theta)\cdot\left[u(\theta)-u(\theta-\theta_{env})\right]}}\right)\Leftrightarrow$$

$$\Leftrightarrow \frac{A}{10} = \log\left(\frac{16\cdot\pi^2\cdot d^{2+\gamma\cdot\cos(\theta)\cdot\left[u(\theta)-u(\theta-\theta_{env})\right]}}{\lambda^2\cdot d_0^{\gamma\cdot\cos(\theta)\cdot\left[u(\theta)-u(\theta-\theta_{env})\right]}}\right)\Leftrightarrow$$

$$\Leftrightarrow \frac{16\cdot\pi^2\cdot d^{2+\gamma\cdot\cos(\theta)\cdot\left[u(\theta)-u(\theta-\theta_{env})\right]}}{\lambda^2\cdot d_0^{\gamma\cdot\cos(\theta)\cdot\left[u(\theta)-u(\theta-\theta_{env})\right]}} = 10^{\frac{A}{10}}\Leftrightarrow$$

$$\Leftrightarrow d^{2+\gamma\cdot\cos(\theta)\cdot\left[u(\theta)-u(\theta-\theta_{env})\right]} = 10^{\frac{A}{10}}\cdot\frac{\lambda^2\cdot d_0^{\gamma\cdot\cos(\theta)\cdot\left[u(\theta)-u(\theta-\theta_{env})\right]}}{16\cdot\pi^2}\Leftrightarrow$$

$$\Leftrightarrow d = \left[10^{\frac{A}{10}}\cdot\frac{\lambda^2\cdot d_0^{\gamma\cdot\cos(\theta)\cdot\left[u(\theta)-u(\theta-\theta_{env})\right]}}{16\cdot\pi^2}\right]^{\frac{1}{2+\gamma\cdot\cos(\theta)\cdot\left[u(\theta)-u(\theta-\theta_{env})\right]}}\Leftrightarrow$$

$$\Leftrightarrow d = \left[10^{\frac{PL-6\cdot\log\left(\frac{f}{2000}\right)\cdot\cos(\theta)\cdot\left[u(\theta)-u(\theta-\theta_{env})\right]-s\cdot\cos(\theta)\cdot\left[u(\theta)-u(\theta-\theta_{env})\right]}{10}}\cdot\frac{\lambda^2\cdot d_0^{\gamma\cdot\cos(\theta)\cdot\left[u(\theta)-u(\theta-\theta_{env})\right]}}{16\cdot\pi^2}\right]^{\frac{1}{2+\gamma\cdot\cos(\theta)\cdot\left[u(\theta)-u(\theta-\theta_{env})\right]}}$$

References

[3gpplte-longtermevolution.blogspot.pt, 2012]
http://3gpplte-longtermevolution.blogspot.pt/2010/06/introduction-to-lte.html, accessed in October 2012;

[aerospaceweb.org, 2018]
http://www.aerospaceweb.org/question/performance/q0088.shtml, accessed in June 2018;

[airliners.net, 2011]
http://www.airliners.net/aviation-forums/tech_ops/read.main/191106/, accessed in September 2011;

[ana.pt, 2018]
https://www.ana.pt/pt/system/files/documents/relatorio_de_gestao_e_contas_2016_vpt_assinada_05abr2016_vcompactada.pdf, accessed in June, 2018;

[astrosurf.com, 2012]
http://www.astrosurf.com/luxorion/qsl-ham-history3.htm, accessed in October, 2012;

[boeing.com, 2018]
http://www.boeing.com/commercial/747family/pf/pf_400_prod.html, accessed in June 2018;

[businessinsider.com, 2012]
http://www.businessinsider.com/complete-visual-history-of-cell-phones-2011-5?op=1, accessed in October, 2012;

[cisco.com, 2018]
http://www.cisco.com/en/US/solutions/collateral/ns341/ns525/ns537/ns705/ns827/white_paper_c11-520862.html, accessed in June, 2018;

[Crouch, 2004] Crouch, Tom D., *Wings: a history of aviation from kites to the space age*, New York: W. W. Norton & Co., 2004;

[electronicproducts.com, 2012]
http://www2.electronicproducts.com/LTE_Advanced_testing_What_to_expect-article-farc_agilent_jul2011-html.aspx, accessed in October, 2012;

[Eurocontrol, 2018] Eurocontrol, *Annual Network Operations Report 2016*, 2018.
http://www.eurocontrol.int/sites/default/files/publication/files/nm-annual-network-operations-report-2016-main-report.pdf;

[Ghosh *et al.*, 2010] Ghosh, A., Ratasuk, R., Mondal, B., Mangalvedhe, N., Thomas, T., "LTE-Advanced: Next-Generation Wireless Broadband Technology", *IEEE Wireless Communications*, vol. 17, no. 3, pp. 10-22, June 2010;

[Ghosh *et al.*, 2011] Ghosh, A., Ratasuk, R., Essentials of LTE and LTE-A, Cambridge University Press, 2011;
[Grant, 2002] Grant, R. G., *Flight: The complete history*, Dorling Kindersley, 2002;

[Iwamura et al., 2010] Iwamura, M., Etemad, K., Mo-Han, F., Nory, R., Love, R., "Carrier Aggregation Framework in 3GPP LTE-Advanced", *IEEE Communications Magazine*, vol. 48, no. 8, pp. 60-67, August 2010;

[Montenegro-Villacieros *et al.*, 2010] Montenegro-Villacieros, B., Oestges, C., Vanhoenacker-Janvier, D., Prieto-Cerdeira, R., Martellucci, A., 2010, "Review and Update of Mobile Data Processing For the Land Mobile Satellite Channel Modeling", *4th European Conference on Antennas and Propagation (EuCAP)*;

[netseminar.stanford.edu, 2012]
http://netseminar.stanford.edu/seminars/01_29_09.pdf, accessed in January, 2012;

[openflights.org, 2018]
http://openflights.org/data.html, accessed in June 2018;

[physicsforums.com, 2011]
http://www.physicsforums.com/showthread.php?t=172045, accessed in September, 2011;

[radio-electronics.com, 2012]
http://www.radio-electronics.com/info/cellulartelecomms/lte-long-term-evolution/3g-lte-basics.php, accessed in August, 2012;

[Rappaport, 2002] Rappaport, Theodore S., 2002, *Wireless Communications Principles and Practice 2nd Edition*, Prentice-Hall;

[Rohde & Schwarz, 2012] UMTS Long Term Evolution (LTE) Technology Introduction, Rohde & Schwarz, 2012;

[Salema, 2002] Salema, Carlos, 2002, *Feixes Hertzianos*, Lisboa: IST Editora;

[Sesia *et al.*, 2009] Sesia, S., Toufik, I., Baker, M., 2009, *LTE – The UMTS Long Term Evolution – From theory to practice*, Wiley;

[Stacey, 2008] Stacey, Dale, *Aeronautical Radio Communication Systems and Networks*, Wiley, 2008;

[telegraph-history.org, 2012]
http://www.telegraph-history.org/samuel-morse/signature.html, accessed in October, 2012;

[Varela, 2009] Varela, F. F., 2009, *Desenvolvimento de um modelo de propagação unificado para o planeamento de redes Wi-Fi, UMTS e WiMAX*, Dissertação de Mestrado em Engenharia de Telecomunicações e Informática, ISCTE-IUL, Lisboa;

[Vieira, 2005] Vieira, Pedro, 2005, *Folhas Teóricas da Unidade Curricular "Planeamento de Redes Móveis - Capítulo 2 - Modelos de Propagação*, Departamento de Engenharia de Electrónica e Telecomunicações e de Informática, ISEL, Lisboa;

[virtualskies.arc.nasa.gov, 2011]
http://virtualskies.arc.nasa.gov/navigation/6.html, accessed in September 2011;

[wikipedia.org, 2011a]
http://en.wikipedia.org/wiki/File:World-airline-routemap-2009.png, accessed in September 2011;

[wikipedia.org, 2011b]
http://en.wikipedia.org/wiki/Descent_%28aircraft%29, accessed in September 2011;

[wikipedia.org, 2011c]
http://en.wikipedia.org/wiki/Final_approach_%28aviation%29, accessed in September 2011;

[wikipedia.org, 2012]
http://en.wikipedia.org/wiki/Friis_transmission_equation, accessed in August, 2012;

[wikipedia.org, 2018a]
https://en.wikipedia.org/wiki/Global_Internet_usage#/media/File:InternetPenetrationWorldMap.svg, accessed in June 2018;

[wikipedia.org, 2018b]
http://en.wikipedia.org/wiki/World%27s_busiest_airports_by_passenger_traffic, accessed in June 2018.